HHS Public Access

Author manuscript

Cell Rep. Author manuscript; available in PMC 2024 July 02.

Published in final edited form as:

Cell Rep. 2024 May 28; 43(5): 114149. doi:10.1016/j.celrep.2024.114149.

Thbs1 regulates skeletal muscle mass in a TGFβ-Smad2/3-ATF4-dependent manner

Davy Vanhoutte[1], **Tobias G. Schips**[1,3], **Rachel A. Minerath**[1], **Jiuzhou Huo**[1], **Naga Swathi Sree Kavuri**[1], **Vikram Prasad**[1], **Suh-Chin Lin**[1], **Michael J. Bround**[1], **Michelle A. Sargent**[1], **Christopher M. Adams**[2], **Jeffery D. Molkentin**[1,4,*]

[1]Department of Pediatrics, University of Cincinnati, Cincinnati Children's Hospital Medical Center, Cincinnati, OH 45229, USA

[2]Division of Endocrinology, Metabolism and Nutrition, Department of Medicine, Mayo Clinic, Rochester, MN 55905, USA

[3]Present address: Janssen Pharmaceuticals, Spring House, PA 19577, USA

[4]Lead contact

SUMMARY

Loss of muscle mass is a feature of chronic illness and aging. Here, we report that skeletal muscle-specific thrombospondin-1 transgenic mice (Thbs1 Tg) have profound muscle atrophy with age-dependent decreases in exercise capacity and premature lethality. Mechanistically, Thbs1 activates transforming growth factor β (TGFβ)-Smad2/3 signaling, which also induces activating transcription factor 4 (ATF4) expression that together modulates the autophagy-lysosomal pathway (ALP) and ubiquitin-proteasome system (UPS) to facilitate muscle atrophy. Indeed, myofiber-specific inhibition of TGFβ-receptor signaling represses the induction of ATF4, normalizes ALP and UPS, and partially restores muscle mass in Thbs1 Tg mice. Similarly, myofiber-specific deletion of *Smad2* and *Smad3* or the *Atf4* gene antagonizes Thbs1-induced muscle atrophy. More importantly, *Thbs1*$^{-/-}$ mice show significantly reduced levels of denervation- and caloric restriction-mediated muscle atrophy, along with blunted TGFβ-Smad3-ATF4 signaling. Thus, Thbs1-mediated TGFβ-Smad3-ATF4 signaling in skeletal muscle regulates tissue rarefaction, suggesting a target for atrophy-based muscle diseases and sarcopenia with aging.

In brief

*Correspondence: jeff.molkentin@cchmc.org.

AUTHOR CONTRIBUTIONS

Conceptualization, D.V. and J.D.M.; methodology, D.V., T.G.S., R.A.M., J.H., and M.A.S.; investigation, D.V., T.G.S., R.A.M., V.P., J.H., N.S.S.K., S.-C.L., M.J.B., and M.A.S.; formal analysis, D.V., T.G.S., R.A.M., V.P., J.H., N.S.S.K, M.J.B., and M.A.S.; writing – original draft, D.V. and J.D.M.; writing – reviewing & editing, D.V. and J.D.M.; funding acquisition, J.D.M.; resources, C.M.A.; supervision, D.V. and J.D.M.

DECLARATION OF INTERESTS

The authors declare no competing interests.

SUPPLEMENTAL INFORMATION

Supplemental information can be found online at https://doi.org/10.1016/j.celrep.2024.114149.

Vanhoutte et al. show that Thbs1 is induced with skeletal muscle atrophy and that Thbs1 directly incites skeletal muscle wasting by modulating autophagy and ubiquitin-proteosome activity. Thbs1-null mice are partially protected from denervation- and starvation-induced muscle atrophy. Mechanistically, Thbs1 facilitates TGFβ-Smad2/3 signaling and ATF4 expression to mediate muscle atrophy.

Graphical Abstract:

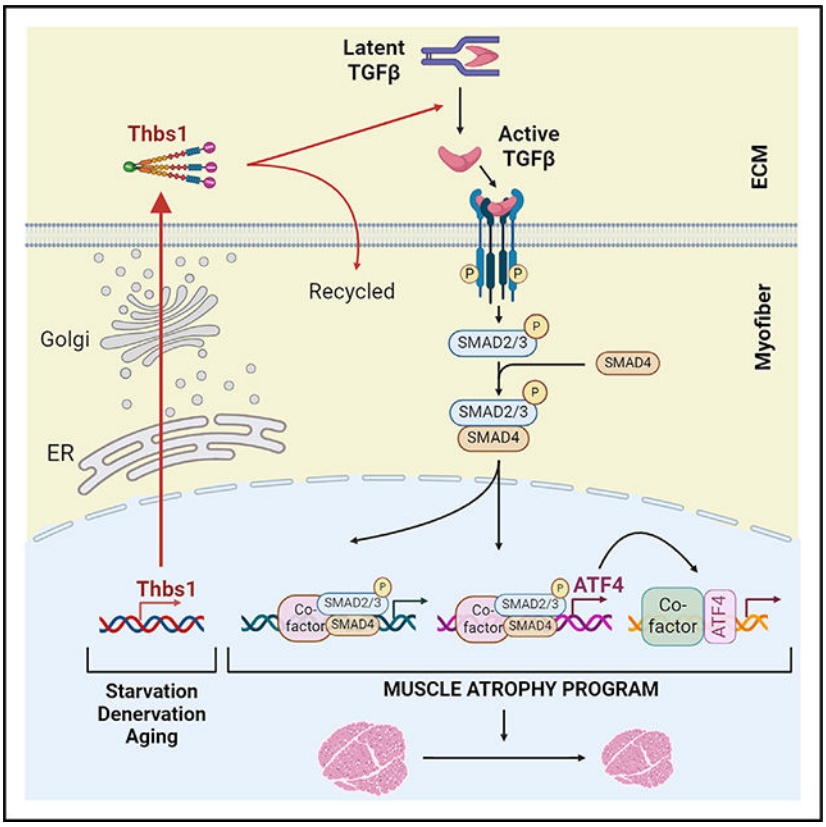

INTRODUCTION

Skeletal muscle atrophy contributes to the morbidity and mortality of a wide array of catabolic conditions, including myopathies, starvation, cancer, heart failure, and age-related sarcopenia.[1,2] The ubiquitin-proteasome system (UPS) and the autophagy-lysosome pathway (ALP) represent the two major proteolytic mechanisms in skeletal muscle that underlie muscle mass loss, which are regulated through a growing number of signaling pathways.[3] Classical signaling pathways that control muscle mass include activation of the insulin- and insulin-like growth factor 1 (IGF1)-induced protein kinase B (AKT)/mechanistic target of rapamycin (mTOR) signaling, which promote growth while simultaneously inhibiting UPS and autophagy to prevent protein breakdown.[4,5] In contrast, transforming growth factor β (TGFβ) and its closely related family members activin, growth and differentiation factor 11 (GDF11), and myostatin (GDF8) promote muscle wasting through phosphorylation of Smad2/3 transcription factors which then induce genes that can

drive these processes.[6–14] Studies have determined that the unfolded protein response and endoplasmic reticulum (ER) stress pathways can also underlie muscle atrophy.[15] Notably, activating transcription factor 4 (ATF4), which is activated by the protein kinase R (PKR)-like ER kinase (PERK) arm of the ER stress pathway, is involved in skeletal muscle wasting due to unloading, fasting, and aging.[16–20] Despite growing efforts, the proximal signaling events that control these pathways remain poorly understood.

Thrombospondins are a family of five multifunctional glycoproteins in mammals.[21] Although traditionally characterized as secreted matricellular proteins, studies have revealed that thrombospondins can also function as intracellular chaperones that mediate ER stress-related pathways, facilitate secretory pathway activity and extracellular matrix (ECM) deposition, and the residence of cellular attachment integrin complexes at the cell membrane.[22–26] The thrombospondin (Thbs) family is subdivided into two groups depending on their sequence conservation and oligomeric structure; subgroup A consists of Thbs1 and Thbs2, while subgroup B consists of Thbs3, Thbs4, and Thbs5.[21] While each Thbs family member is expressed in select tissues during early development, their expression is typically silenced in adult tissues and only observed with injury or stress stimulation.[27] For example, Thbs1 induction within the heart during stress was recently shown to induce cardiomyocyte atrophy, a function that is not shared with any of the other Thbs family members.[22,25,26] Endogenous Thbs1 induction or its transgenic overexpression was mechanistically linked to activation of the PERK-ATF4 ER-stress axis, leading to autophagy and lethal atrophic cardiomyopathy that was blocked by deletion of the gene encoding PERK (*Eif2ak3*). Moreover, mice lacking endogenous *Thbs1* developed greater cardiac hypertrophy with pressure-overload stimulation and were protected against fasting-induced cardiac atrophy.[26] Consistent with these findings, two independent studies showed that Thbs1 protein is induced in atrophied rat soleus due to hindlimb unloading.[28,29] Thbs1 is also upregulated during paravertebral muscle atrophy in patients with adult degenerative scoliosis,[30] together suggesting a broader physiological role for Thbs1 in regulating muscle atrophy.

Here we show that expression of Thbs1, but not other Thbs family members, is induced in skeletal muscle by stimuli that cause atrophy, and that Thbs1 overexpression selectively facilitates profound muscle atrophy by inducing myofiber-specific TGFβ-Smad2/3 signaling that is independent of PERK, resulting in ATF4 activation and altered UPS- and ALP-mediated muscle proteolysis. Moreover, targeted deletion of *Thbs1* significantly attenuates denervation- and fasting-induced skeletal muscle atrophy. Altogether, our findings establish Thbs1-TGFβ-Smad2/3-ATF4 signaling as a previously unrecognized yet fundamental mediator of skeletal muscle mass and health.

RESULTS

Thbs1 is induced in mouse models of skeletal muscle atrophy

Thbs1 was shown to reduce cardiomyocyte size in the stressed heart, and its expression is induced in atrophied rat soleus due to hindlimb unloading and during human paravertebral muscle atrophy in adult degenerative scoliosis.[26,28–30] Indeed, analysis of published microarray data (GEO: GSE80223) in the public domain revealed increased *Thbs1* gene

expression in atrophied soleus of space-flown mice (Figure 1A). *Thbs1* mRNA expression was also induced as early as 3 days and remained elevated at day 6 following unilateral sciatic nerve denervation in tibialis anterior (TA), whereas the expression of Thbs2, Thbs3, Thbs4, and Thbs5 remained unaltered (Figure 1B). Western blot analysis and immunostaining revealed that Thbs1 was undetectable in control TA yet induced in denervated atrophic TA, where it primarily co-localized with the ER marker BiP (binding immunoglobulin protein) inside the myofiber (Figures 1C and 1D). Similarly, Thbs1 mRNA and/or protein was also induced in TA and quadriceps of mice subjected to 48 h of fasting and with old age (Figures 1E–1G), with protein localization primarily inside the ER compartment of the aged myofiber (Figure 1H). Together, these results suggest that induction of endogenous Thbs1 expression might underlie striated muscle atrophy or sarcopenia.

Skeletal muscle-specific overexpression of Thbs1 induces muscle atrophy

To test the hypothesis that Thbs1 underlies skeletal muscle atrophy, we generated transgenic (Tg) mice that selectively overexpress Thbs1 in skeletal muscle using the skeletal α-actin promoter, which produced abundant protein overexpression at 6 and 52 weeks of age (Figures 2A and 2B). Immunohistochemistry and biochemical analyses revealed that the transgene was abundantly expressed and co-localized with BiP within the ER vesicular network on the inside periphery of the myofiber as well as partially outside the myofiber with the collagen-I-containing ECM, although Thbs1 was not observed in the circulation in plasma (Figures 2C, 2D, S1A, and S1B). In parallel, adenoviral-mediated overexpression of Thbs1 augments rates of intracellular vesicular trafficking between the ER, Golgi, and sarcolemma in neonatal rat ventricular myocytes (NRVMs), and Thbs1 Tg mice showed greater sarcolemmal residency β-dystroglycan, δ-sarcoglycan, α-sarcoglycan, β-sarcoglycan, and β1D-integrin within the quadriceps compared to Ntg controls (Figures S1C–S1E). Therefore, Thbs1 expression in skeletal muscle appears to function as an ER chaperone, as we showed previously for Thbs4.[23,24]

Strikingly, Thbs1 Tg mice displayed a profound reduction in skeletal muscle mass (quadriceps, gastrocnemius, and diaphragm) compared to Ntg littermate controls without a change in tibia length at multiple ages (Figures 2E–2G and S1F–S1H). Myofiber cell surface area was significantly smaller with overexpression of Thbs1, and functional analyses revealed that Thbs1 Tg mice had progressively reduced running ability on a treadmill and significantly weaker grip strength normalized to body weight over time, as well as a shortened lifespan versus Ntg controls (Figures 2H–2L).

To address the potential independent effect of the Thbs1 transgene on postnatal skeletal muscle growth, we also evaluated whether timed overexpression of Thbs1 can induce skeletal muscle atrophy in adult mice. Adeno-associated virus (MyoAAV)-mediated overexpression of either Thbs1 or luciferase (control) was performed in the gastrocnemius of 8-week-old wild-type (WT) mice (Figures S2A and S2B). Six weeks later, MyoAAV-mediated overexpression of Thbs1 resulted in atrophic remodeling of the gastrocnemius as shown by reduced muscle weight and reduced cell surface area of infected, Thbs1-positive myofibers versus the neighboring uninfected myofibers, as determined by Thbs1

immunohistochemistry (Figures S2C–S2E). Collectively, these data confirmed that Thbs1 is sufficient to induce skeletal muscle atrophy in adulthood.

Previous literature has suggested that Thbs1 induction could underlie capillary regression in unloaded atrophied skeletal muscle.[28,29] However, sustained overexpression of Thbs1 in quadriceps had no effect on capillary density (Figure S2F). Thbs1 Tg mice also did not show overt signs of muscle pathology such as fibrosis or myofiber regeneration with embryonic myosin expression (eMyHC) (Figures 2G, 2H, and S2G). Taken together, these results indicate that Thbs1 induces skeletal muscle atrophy when overexpressed *in vivo* but does not otherwise cause overt muscle histopathology.

Thbs1 induces PERK, ATF4, and protein degradation in skeletal muscle

Recently we showed that Thbs1 induction in the heart was a strong mediator of atrophy through an ER stress-dependent pathway involving PERK-induced autophagy.[26] Hence, we performed comparative ER stress analysis by western blot in Thbs1 Tg quadriceps, as compared to quadriceps of mice with skeletal muscle-specific Thbs4 or ATF6α overexpression (Thbs4 Tg and ATF6α Tg, respectively) and Ntg controls at 6 weeks of age (Figure 3A). Thbs4 Tg and ATF6α Tg mice did not show a change in tibia length, body weight, or muscle weight at 6 weeks of age compared with Ntg mice, while Thbs1 Tg mice displayed skeletal muscle atrophy (Figures S3A–S3E). While Thbs1, Thbs4, and ATF6α transgenic quadriceps all showed induction of nuclear ATF6α (ATF6α-N) and ER resident chaperones BiP and calreticulin, Thbs1 uniquely induced PERK, ATF4, and its downstream target fibroblast growth factor 21 (FGF21; Figure 3A). Notably, Thbs1 overexpression also enhanced levels of inositol-requiring 1α (Ire1α) in skeletal muscle, like ATF6α Tg mice (Figure 3A). Moreover, autophagy and lysosomal markers were uniquely altered in muscle from Thbs1 Tg mice, such as microtubule-associated proteins 1A/1B light chain 3b (LC3b-II), p62, lysosomal-associated membrane protein 1 (LAMP1), LAMP2, and lysosomal integral membrane protein II (LIMPII) (Figure 3A). To investigate altered autophagic flux suggested by the western blotting profile, Thbs1 Tg animals and Ntg controls were treated with colchicine, a microtubule-depolymerizing agent that inhibits autophagosome-lysosome fusion.[32] Interestingly, colchicine did not further increase in LC3b-II levels in Thbs1 Tg quadriceps, suggesting an impaired ALP with overexpression of Thbs1 (Figures 3B and 3C; see discussion). In contrast, activity of the 20S proteasome and levels of ubiquitinated proteins were selectively increased in Thbs1 Tg quadriceps but not in Thbs4 Tg and ATF6α Tg compared to Ntg control quadriceps (Figures 3D, 3E, and S4A). Interestingly, this profound atrophy due to Thbs1 overexpression also enhanced the rate of protein synthesis in the same muscle (Figures S4B and S4C). Ultrastructural analyses by transmission electron microscopy from Thbs1 Tg quadriceps revealed areas of disorganized sarcomeres with abundant autophagosome- and lysosome-like vesicular structures (Figure S4D). Collectively, these findings indicate that Thbs1 impairs the ALP and enhances the activity of the UPS protein degradation pathways in skeletal muscle, consistent with the observed atrophic effect.

As an additional control, we also generated skeletal muscle-specific transgenic mice overexpressing Thbs1's most related family member, Thbs2,[21] which also showed abundant

protein overexpression in muscle (Figure 3F). Interestingly, overexpression of Thbs2 did not induce ATF6α-N, PERK, ATF4, or the lysosomal marker LAMP2, nor did it cause loss of muscle mass or a reduction in myofiber cell surface area (Figures 3F–3H and S3A–S3E).

Finally, previous studies have associated the PERK-ATF4 ER stress axis with increased expression of mTORC1 inhibitors, sestrin 2 (SSN2), and DNA-damage-inducible transcript 4 (DDIT4).[33,34] At the same time, ATF4 was also shown to inhibit the activity of the AKT/mTORC1 pathway through upregulation of DDIT3/tribbles pseudokinase 3 (TRIB3).[2,34,35] While we did not observe effects of Thbs1 overexpression on the phosphorylation of mTOR, P70 S6K, AMPKα, AKT, FoxO1, or FoxO3, the levels of phosphorylated 4E-BP1 appeared to be increased in Thbs1 Tg quadriceps compared to Ntg control (Figure S4E). Taken together, these findings suggest that Thbs1-induced muscle atrophy is associated with enhanced mTORC1/4E-BP1-regulated protein translation.

Thbs1-mediated muscle atrophy is independent of PERK, ATF6α, CD47, and CD36

We previously observed that deletion of the gene encoding PERK protein (*Eif2ak3*) in the heart normalized the levels of ATF4 induction and autophagy as well as antagonizing the lethal cardiac atrophy due to cardiac-specific Thbs1 overexpression.[26] However, genetic deletion of *Eif2ak3* in skeletal muscle did not antagonize Thbs1-dependent atrophy, nor did it normalize the downstream molecular effector pathways associated with autophagy (Figures 4A–4D). Specifically, Thbs1 Tg mice were crossed with *Eif2ak3*-LoxP(fl)-targeted (*Eif2ak3*$^{fl/fl}$) mice and skeletal muscle-specific *Myl1*-cre gene-targeted mice (cre inserted into the myosin light chain 1/3 locus[36]; Figure 4A). Deletion of *Eif2ak3* from skeletal muscle, confirmed by western blotting, did not normalize protein levels of ATF4, FGF21, LC3b-I/II, p62, LAMP1, LAMP2, and LIMPII, nor did it prevent loss of skeletal muscle mass induced by the Thbs1 transgene at 12 weeks of age (Figures 4B–4D and S5A–S5C). Hence, PERK does not regulate Thbs1-induced atrophy in skeletal muscle, in contrast to our previous observations in the heart.[26]

ER stress effector ATF6α and cell-surface receptors CD36 and CD47 were previously identified as interactors and direct effectors of Thbs1.[21,22,37] Although ATF6α, CD36, and CD47 are known to have dominant functions independent of Thbs1,[38–40] we examined whether they contributed to the Thbs1-mediated muscle atrophy. Hence, *Atf6*$^{-/-}$, *Cd36*$^{-/-}$, or *Cd47*$^{-/-}$ mice were crossed into the Thbs1 muscle-specific transgene background, which showed that loss of *Atf6*, *Cd36*, or *Cd47* had no effect on the degree of Thbs1-induced muscle atrophy (Figures 4E–4G and S5D–S5F). In fact, loss of ATF6α appeared to further exaggerate the decrease in muscle mass and induced fibrotic remodeling in Thbs1 Tg quadriceps. In conclusion, PERK, ATF6α, CD47, and CD36 have no direct role in facilitating Thbs1-mediated skeletal muscle atrophy.

Thbs1 activates TGFβ-Smad3-ATF4 signaling to facilitate skeletal muscle atrophy

To examine the potential molecular mechanism whereby Thbs1 induces skeletal muscle atrophy, we performed global RNA sequencing on quadriceps at 6 weeks of age from Thbs1 Tg and Ntg mice, which revealed a signature of enhanced TGFβ signaling (Figure 5A). Canonical TGFβ-Smad2/3 signaling is a primary pathway controlling muscle mass,[6–11]

while Thbs1 was previously recognized as a major regulator of latent TGFβ activation.[41–43] Indeed, endogenous TGFβ activity and downstream phosphorylation of Smad3 were markedly enhanced in Thbs1 Tg quadriceps but not in Thbs2, Thbs4 Tg, and ATF6α Tg quadriceps compared to Ntg controls at 6 weeks of age (Figures 5B–5D). Consistent with these findings, increased immunostaining of nuclear phospho-Smad2/3 was detected in myofibers of Thbs1 Tg quadriceps versus Ntg controls (Figure S6A), while a cell-based assay confirmed greater levels of active TGFβ within the ECM of quadriceps from Thbs1 Tg mice compared to ECM from Ntg controls (Figure S6B).

A Smad3-dependent crosstalk between ATF4 and TGFβ was recently identified in triple-negative breast cancer and brown adipose tissue.[44,45] Here, Smad3 was shown to directly bind to the *Atf4* promoter region independent of PERK in regulating *Atf4* transcription.[44,45] These observations in combination with our findings encouraged us to examine whether TGFβ-Smad3-signaling might also induce ATF4 independent of PERK. To examine this, mouse embryonic fibroblasts (MEFs) were isolated from embryonic day 13.5 *Eif2ak3*$^{fl/fl}$ (PERK) embryos, transduced with an adenovirus encoding cre recombinase (Adcre) and compared to Adβgal-injected controls. Two days later, cells were treated with 10 ng/mL TGFβ for 6 h (Figure S6C). The results show that deletion of the gene encoding PERK did not reduce phospho-Smad3 or ATF4 induction in response to TGFβ stimulation (Figure S6C). Indeed, overexpression of Smad3 was sufficient to induce ATF4, with or without the presence of PERK (Figure S6D). Hence, TGFβ and canonical TGFβ-mediated Smad3 signaling can induce ATF4 in a PERK-independent manner.

While a role for Smad2/3 and ATF4 in skeletal muscle atrophy have previously been reported,[2,10,17] a direct mechanistic link between Thbs1, TGFβ-Smad2/3, and ATF4 in regulating skeletal muscle atrophy has not been established. As a potential mechanism, Thbs1 binds and activates latent TGFβ through the KRFK sequence located in the Thbs1 type-1 repeats, which is missing from Thbs2.[42,43,46,47] Hence, here we generated adenoviruses that harbor full-length Thbs1 or a Thbs1Δt1 mutant that is devoid of the Thbs1 type-1 repeat domain (Figure 5E). Utilizing recombinant adenoviruses in cultured NRVMs, we confirmed that full-length Thbs1 and mutant Thbs1Δt1 are expressed and secreted into the media with at least the same efficiency (Figures S6E and S6F). More importantly, while adenoviral-mediated overexpression of full-length Thbs1 in the gastrocnemius of neonatal rat pups induced ATF4 and reduced the mass and myofiber cell surface area by 16 days of age as compared to Adβgal-injected controls, overexpression of the Thbs1Δt1 mutant did not (Figures 5F–5H and S6G). No overt signs of other histopathological changes, including a potential inflammatory response, were observed (Figure S6G).

Next, we crossed Thbs1 Tg mice with skeletal muscle-specific transgenic mice that express a TGFβ type II receptor dominant-negative truncation mutant (dnTGFβRII Tg) to block TGFβ signaling specifically at the level of the myofiber.[48] Strikingly, we observed that expression of the dnTGFβRII transgene in Thbs1 Tg muscle (DTg) not only inhibited the phosphorylation of Smad3 but also blunted the induction of ATF4 and nearly normalized autophagy and lysosomal markers LC3b-I/II, p62, LAMP1, LAMP2, and LIMPII, as well as 20S proteasome activity at 12 weeks of age, compared to Ntg and dnTGFβRII Tg controls (Figures 5I, S7A, and S7B). In addition, myofiber-specific inhibition of TGFβ signaling

antagonized the reduction in myofiber cross-sectional area at 3 months of age and the loss of skeletal muscle mass at 3 and 6 months of age due to the overexpression of Thbs1 (Figures 5J, 5K, S7C, and S7D). Collectively, these data provide genetic evidence that Thbs1-mediated TGFβ signaling is critical in driving skeletal muscle atrophy.

Smad2/3 and downstream ATF4 mediate Thbs1-induced muscle atrophy

To further examine the mechanistic link between Thbs1, TGFβ-Smad2/3, ATF4, and skeletal muscle atrophy, we crossed *Smad2/3*$^{fl/fl}$ targeted mice with *Myl1*-cre mice to establish a myofiber-specific deletion of *Smad2/3* (*Smad2/3*^{mKO}) in the presence of the Thbs1 transgene (Thbs1 Tg *Smad2/3*^{mKO}). Myofiber-specific deletion of *Smad2/3* blunted the induction of ATF4 and normalized levels of FGF21, LC3b-I/II, p62, LAMP2, and LIMPII, as well as 20S proteasome activity and the levels of ubiquitinated proteins in Thbs1 Tg skeletal muscle at 12 weeks of age (Figures 6A, 6B, S7E, and S7F). Importantly, deletion of *Smad2/3* significantly rescued the loss of muscle mass due to overexpression of Thbs1 at 12 weeks of age (Figures 6C and S7G).

Consistent with these observations, direct adenoviral-mediated overexpression Smad3 (AdSmad3) in the gastrocnemius of neonatal rat pups induced pSmad3 levels and ATF4, resulting in atrophy of this muscle by 16 days of age as compared to Adβ gal-injected controls (Figures 6D and 6E). Using a similar experimental approach, we also showed that inhibition of the canonical TGFβ pathway by adenoviral-mediated overexpression of the inhibitory Smad6 and Smad7 proteins was sufficient to inhibit AdThbs1-mediated decrease in gastrocnemius mass (Figure 6F).

Finally, we generated mice with myofiber-specific deletion of *Atf4* (*Atf4*$^{fl/fl}$-*Myl1*-cre mice; *Atf4*^{mKO}) and crossed them into the Thbs1 Tg genetic background (Thbs1 Tg; *Atf4*^{mKO}). Deletion of *Atf4* in muscles of Thbs1 Tg mice blunted the induction of ATF4 protein and its target FGF21 and normalized the levels of LC3b-I/II, p62, LAMP2, and 20S proteasome activity compared to control littermates (Figures 6G and 6H). More importantly, deletion of *Atf4* also significantly antagonized the loss of muscle mass induced by Thbs1 overexpression (Figures 6I and S7H). These results indicate that Thbs1-induced activation of TGFβ-Smad2/3 signaling functions, in part, upstream of ATF4 in facilitating muscle atrophy.

Loss of *Thbs1* prevents denervation- and fasting-induced muscle atrophy

To directly investigate the physiological relevance of Thbs1 as an endogenous inducer of muscle atrophy, we examined *Thbs1*$^{-/-}$ mice. These mice were subjected to denervation-induced muscle atrophy of the right hindlimb, while the left hindlimb served as a sham-operated internal control. Strikingly, denervation-induced phosphorylation of Smad2 and induction of ATF4, LC3b-I/II, p62, LAMP1, LAMP2, and LIMPII in the TA were all antagonized in *Thbs1*$^{-/-}$ mice 10 days post surgery compared to sham-operated controls (Figure 7A). The absence of the *Thbs1* gene also significantly antagonized the reduction in muscle mass and loss of myofiber cell surface area that occurred 10 days after denervation as compared to WT controls (Figures 7B and 7C). As a control, myofiber-specific inhibition of TGFβ signaling also significantly reduced denervation-induced loss of muscle mass,

whereas the absence of Thbs4 did not (Figures 7D and 7E). Taken together, these data support the hypothesis that induction of endogenous Thbs1 is a physiological mediator of skeletal muscle atrophy due to denervation.

We also assessed whether *Thbs1*$^{-/-}$ mice were resistant to fasting-induced skeletal muscle atrophy. The results show that loss of TA mass and reduced myofiber cell surface area with 48 h of fasting were significantly blunted in the absence of *Thbs1* compared to WT control mice (Figures 7F and 7G). In contrast, *Thbs1*$^{-/-}$ mice were not protected against fasting-induced loss in liver weight(Figure 7H), suggesting muscle specificity. As a further control, we observed that genetic deletion of *Thbs4* did not attenuate fasting-induced loss in TA mass nor antagonize the loss of myofiber cross-sectional area (Figures 7I and 7J). Collectively, these results suggest that the induction of endogenous Thbs1 is required for caloric restriction-induced skeletal muscle atrophy.

DISCUSSION

While previous studies identified Thbs1 as an activator of TGFβ,[42,43] and it was known that TGFβ signaling and ATF4 can drive skeletal muscle atrophy,[6–11,49] the current study shows that Thbs1 regulates TGFβ-Smad2/3-ATF4 signaling to drive skeletal muscle rarefaction. Our findings support a model whereby mechanical and nutritional stresses trigger the expression of Thbs1 in the myofiber, which then facilitates muscle atrophy by activating TGFβ and promoting myofiber-specific TGFβ-Smad2/3 signaling with downstream induction of pro-atrophic ATF4 expression. Indeed, deletion of *Thbs1* in mice blunted this pathway and diminished denervation- and fasting-induced skeletal muscle atrophy, suggesting that Thbs1 is a required endogenous mediator of muscle atrophy and that the transgenic overexpression approach revealed the true biological function of Thbs1.

In other cell types, Thbs1 can activate TGFβ by triggering its dissociation from the small latent complex through a mechanism that involves the KRFK motif that is located in its type-1 repeat domain of Thbs1, which interacts with the LSKL sequence in the latency-associated peptide.[43,47,50,51] Consistent with these past results, here we observed that a mutant form of Thbs1 lacking the type-1 repeat region did not induce ATF4 expression and a reduction in skeletal muscle mass. Moreover, skeletal muscle-specific overexpression of Thbs2, which is highly homologous to Thbs1 but lacks the KRFK sequence,[46,47] or Thbs4, which lacks the entire type-1 domain,[21] also do not activate TGFβ-Smad2/3 signaling, nor do they cause muscle atrophy.

ATF4 appears to be a common effector of Thbs1 in both heart and skeletal muscle. Indeed, previous work from our lab revealed that Thbs1-mediated activation of the canonical PERK-ATF4 ER-stress axis in cardiomyocytes selectively induced autophagy and lysosomal protein degradation and, ultimately, atrophic cardiomyopathy.[26] Here, muscle-specific deletion of *Atf4* protected against starvation-, immobilization-, and age-related muscle atrophy and weakness.[16,17,20,52] While we observe that Thbs1 also induces ATF4 in the myofiber, our results differ from those in the heart in that we failed to blunt the induction of ATF4 and the atrophic phenotype by deletion of the *Eif2ak3* gene (PERK protein).[26] Instead, Thbs1 induces ATF4 though TGFβ-Smad2/3 signaling in the myofiber, independent

of PERK. These findings are supported by previous studies in triple-negative breast cancer cells and mouse adipocytes that show that Smad3 can directly bind to the *Atf4* promoter region and regulate *Atf4* transcription,[44,45] while we showed that active TGFβ and Smad3 signaling can induce ATF4 in *Eif2ak3*-deleted MEFs and that overexpression of Smad3 in the gastrocnemius was sufficient to induce ATF4 and loss of muscle mass. More importantly, myofiber-specific inhibition of TGFβ-receptor signaling or deletion of *Smad2* and *Smad3* prevented the induction of ATF4 and largely corrected the atrophic phenotype observed in Thbs1 Tg muscle, suggesting a direct causal relationship. Finally, cardiomyocyte-specific Thbs1-overexpressing transgenic mice lacking the type-1 repeats that bind TGFβ still caused a lethal atrophic cardiomyopathy,[26] yet in skeletal muscle this mutant form of Thbs1 no longer induced atrophy, indicating that Thbs1 regulates atrophy differently in heart versus skeletal muscle.

Our study also suggests that Thbs1 might be a viable therapeutic target to control TGFβ-Smad2/3-ATF4 signaling and prevent muscle wasting associated with a variety of diseases or unhealthy aging. For example, a selective Thbs1 antagonist for TGFβ atrophic signaling, such as LSKL-containing peptide or the memetic SRI31277, which inhibits Thbs1-TGFβ activation, might represent such an opportunity and could be examined in the future.[42] Alternatively, defining the molecular mechanisms that drive the expression and secretion of Thbs1 itself could help develop specific therapeutic strategies to preserve muscle mass during disease and improve the quality of life during aging.

Limitations of the study

Our results show that Thbs1-mediated skeletal muscle atrophy is independent of PERK signaling but instead signals through TGFβ and Smad2/3, while Thbs1-dependent lethal atrophy in the heart relies on PERK-ATF4 signaling, but not TGFβ. One could argue the implausibility of Thbs1 directly regulating atrophy of both tissue types through completely different mechanisms. However, TGFβ overexpression in the heart does not cause atrophy but instead mediates a small degree of hypertrophy with aging.[53] Also, deletion of the two TGFβ receptors on cardiomyocytes in mice did not overtly affect growth of the heart, nor did a TGFβ blocking monoclonal antibody.[54] Importantly, skeletal muscle is profoundly sensitive to atrophy induced by TGFβ signaling, which extends to other TGFβ superfamily members such as the activins, GDF8, and GDF11.[2,55] Unfortunately, we did not extend our analysis in skeletal muscle to these other TGFβ superfamily members, but it is likely that other effectors also co-regulate Thbs1-induced atrophy, which might explain why deletion of *Smad2/3* genes had greater protection from atrophy than did deletion of *Atf4*. Another limitation of our study is in directly linking Thbs1 to the observed alterations in ALP and UPS and how these processes are differentially regulated by Thbs1 in heart and skeletal muscle. Thbs1-mediated PERK-ATF4 signaling promotes cardiac atrophy by inducing ALP but not UPS,[26] while Thbs1-mediated skeletal muscle atrophy appears to be associated with impaired autophagy and enhanced UPS. Both hyperactivity and impairment of the ALP results in skeletal muscle atrophy.[56–59] Furthermore, suppression of autophagy by muscle-specific deletion of *Atg7* induces a compensatory upregulation of the proteasome system.[58] Similarly, while we showed that Thbs1 induces Smad2/3 and ATF4 signaling directly in skeletal muscle, which itself could underlie induction of some autophagic genes,[60–62]

Thbs1 also directly binds to LIMPII (SCARB2) that is involved in lysosome formation and processing from the ER compartment where Thbs1 is also present.[63] Thus, future studies will investigate whether Thbs1 directly or indirectly interacts with the ALP and UPS and whether this interaction occurs at the transcriptional, translational, and/or post-translational level.

STAR★METHODS

RESOURCE AVAILABILITY

Lead contact—Further information and requests for resources and reagents should be directed to and will be fulfilled by the lead contact, Jeffery D. Molkentin (Jeff.Molkentin@cchmc.org).

Materials availability—All unique/stable reagents generated in this study are available from the lead contact with completed material transfer agreement.

Data and code availability

- All original data reported in this manuscript will be shared by the lead contact upon request or are included in the original figures or the supplemental information. RNA-sequencing data was deposited in the NCBI Gene Expression Omnibus (Geo) and made publicly available upon manuscript acceptance for publication (GEO: GSE245663). Uncropped western blots are shown in Data S1 supplement. This paper also analyzes existing, publicly available data in Figure 1A. The GEO accession number for this dataset is GEO: GSE80223.
- This paper does not report original code.
- Any additional information required to reanalyze the data reported in this work is available from the lead contact upon request.

EXPERIMENTAL MODEL AND STUDY PARTICIPANT DETAILS

Animals—All animal experiments were approved by the Institutional Animal Care and Use Committee of the Cincinnati Children's Hospital Medical Center (Protocol# IACUC 2016–0069, 2018–0047 and 2019–0047). No human subjects or human tissues were used in this study. The number of mice used in this study reflects the minimum number needed to achieve statistical significance based on experience and previous power analysis. Both sexes of mice were used in equal ratios and all animals were housed at 21–22°C, 40–60% humidity, 12-h light/12-h dark cycle, and unless specified differently below with food and water *ad libitum*. Skeletal muscle-specific transgenic mice for Thbs1, Thbs4, ATF6α, and dnTGFβRII were generated using the modified human skeletal α-actin (Ska) promoter plasmid as previously described.[22,24,48,68] Similarly, full-length mouse Thbs2 cDNA (Horizon Discovery, Cat #MMM1013–202702786) was amplified by PCR and cloned into the *SalI* site of the Ska promoter expressing vector (forward: 5′- GTCGACATGCTCTGGGCACTGGCC-3′, and reverse: 5′- GTCGACCTAGGCATCTCTGCACTCATACTTG-3′).[68] Next, the plasmid backbone was removed and the Ska-Thbs2 fragment was gel purified followed by Elutip-D

column purification (Schleicher and Schuell Bioscience; Dassel, Germany, Cat# 10462617). The final construct was confirmed by DNA sequencing and submitted to the *Cincinnati Children's Hospital Transgenic Animal and Genome Editing Core Facility* for newly-fertilized oocyte injection. Transgenic mice were produced in the FVB/N background. Mice deficient for *Thbs1*, *Thbs4*, *Cd36*, and *Cd47*, (*B6.129S2-Thbs1tm1Hyn/J*, B6.129P2-Thbs4tm1Dgen/J, *B6.129S1-Cd36tm1Mfe/J*, and *B6.129S7-Cd47tm1Fpl/J*), LoxP-targeted for *Eif2ak3* (*Eif2ak3tm1.2Drc/J*) and *C57Bl/6J* were purchased from Jackson Laboratories and maintained on a *C57Bl/6J* background. Gene-deleted mice lacking *Atf6* were obtained from the lab of Kazutoshi Mori (Kyoto University, Kyoto, Japan).[69] Mice lacking the *Sgcd* gene (δ-Sarcoglycan),[70] LoxP-targeted *Smad2/3* mice[64] and LoxP-targeted *Atf4* mice were previously described.[17] *Eif2ak3*-LoxP (abbreviated "fl"), *Smad2/3*-LoxP and *Atf4*-loxP mice were crossed with mice expressing cre recombinase under the control of the myosin light chain 1/3 (*Myl1*-cre)[36] genomic locus to generate mice with myofiber specific protein deletion of either PERK, Smad2/3 or ATF4 (referred to as $Eif2ak3^{mKO}$, $Smad2/3^{mKO}$ mice and $Atf4^{mKO}$ mice). Next, Ska-Thbs1 Tg mice were backcrossed for at least 6 generations into the $Eif2ak3^{mKO}$, $Smad2/3^{mKO}$ mice and $Atf4^{mKO}$ background to generate mice with myofiber specific deletion of *Eif2ak3*, *Smad2/3* or *Atf4*, as well as littermate controls.

Primary cell isolations—Neonatal rat ventricular myocytes (NRVMs) were prepared from 1- to 2-day-old Sprague-Dawley rat pups of both sexes as previously described (Inotiv, Cat# 002).[22] $Eif2ak3^{fl/fl}$ and *C57Bl/6J* mouse embryonic fibroblasts (MEFs) were isolated from embryos in E12.5 as previously described.[66] Briefly, decapitated embryos of both sexes were finely minced using sterile blades and passed through a 10 mL syringe. Tissue and cells were incubated at 37°C for 30 min with 5 mL of 0.25% trypsin-EDTA (Fisher Scientific, Cat# MT25–053-Cl) while shaking. Bovine growth serum (Fisher Scientific, Cat# SH3054103) was added to inhibit the trypsin. MEFs were plated in 150 mm dishes and grown in DMEM/high glucose (Fisher Scientific, Cat# SH30022.01) supplemented with 10% bovine growth serum and 1x penicillin-streptomycin (Corning Life Sciences, Cat# 30–0002-CI) at 37°C in 5% CO_2. MEFs were used for a maximum of eight passages and switched to DMEM/high glucose supplemented with 2% bovine growth serum and 1x penicillin-streptomycin 24 h prior to the treatments described below.

METHOD DETAILS

Thbs1 mRNA expression in space-flown mice—A literature search yielded a publicly available Affymetrix Mouse Genome 430A 2.0 microarray dataset (NCBI GEO Repository, GSE80223) in which Gambara G. et al.[31] compared the gene expression adaptation in soleus from adult *C57Bl/n6* mice that were flown in space aboard the BION-M1 biosatelite for 30 days in orbit ($n = 3$), and from sex- and age-matched control mice that were housed in standard vivarium cages ($n = 3$). Fold change in *Thbs1* mRNA levels were averaged and compared to control using a two-tailed unpaired Student's t-test.

RNA isolation, RNA-sequencing, and RT-qPCR—RNA was extracted from 6-week-old Thbs1 Tg and Ntg control quadriceps from two individual mice per genotype using the RNeasy Fibrous Tissue Kit according to manufacturer's instructions (QIAGEN, Cat# 74704). RNA quality was checked using the Agilent 2100 Bioanalyzer and submitted to

the *University of Cincinnati Sequencing and Genome Analysis Core Laboratory*. RNAseq data were analyzed and *p*-values calculated using a negative binomial statistical model as implemented in DESeq (Bioconductor version: Release (2.14)), meanwhile false discover rates were used to obtain the adjusted *p*-values.[71]

For qPCR assays, cDNA was generated by reverse transcription of 1 μg of purified RNA using Superscript™ III First-Strand Synthesis Kit (Invitrogen, Cat# 18080051) with random hexamer primers according to the manufacturer's instructions. Quantitative real-time PCR was performed using SsoAdvanced Universal SYBR Green Supermix (Bio-Rad, Cat# 1725274) on a CFX96 Touch Real-Time PCR System (Bio-Rad). Target gene expression was normalized to that of *Rpl13* (ribosomal protein L13) and expression in the control conditions was set to 1. Sequences of all qPCR primers used in this study are listed in Table S1.

Denervation- and fasting-induced muscle atrophy—Mouse models of unilateral hindlimb denervation- and fasting-induced muscle atrophy were performed as previously described.[26,65] Briefly, sciatic hindlimb denervation was performed by anesthetizing 8-week-old mice with 2–3% inhaled isoflurane, shaving the hind quarters and making a 0.5 cm incision on the lateral side of the leg. The muscles were then separated, and the sciatic nerve was exposed and lifted with surgical forceps. Next, a 5 mm piece of sciatic nerve was removed, and the incision was closed with surgical staples. The left leg served as sham-operated internal control in which the sciatic nerve was exposed but not cut.[65] For fasting studies, 8-week-old male mice were deprived of food for 48 h with free access to drinking water.[26]

Adenoviruses and cell cultures—Recombinant adenoviruses harboring Thbs1, Smad6, Smad7, eGFP-tagged VSVG-ts045, cre recombinase and β-galactosidase (βgal) were previously generated and validated.[22,24,48,67] Similarly, *Smad3* cDNA was amplified by PCR for insertion into the pShuttle-CMV vector (Agilent Technologies, Cat# 240007) to generate AdSmad3 according to the manufacturer's instructions.[22] The Thbs1Δt1 mutant lacking the Thbs1 type1 repeats was created using the In-Fusion® HD cloning kit (Takara Bio; Cat# 639649) and the previously established pShuttle-CMV-Thbs1 vector.[22]

Depending on the experiment, *Eif2ak3*$^{fl/fl}$ MEFs were either infected with recombinant adenoviruses to overexpress cre recombinase (Adcre) or βgal control (Adβgal) for 48 h, and then treated with 10 ng/mL recombinant mouse TGFβ1 (R&D Systems; Cat# 7666-MB-005) for 6 h or infected with Adβgal or Adcre for 24 h, and subsequently infected with Adβgal or AdSmad3 for 24 h. To assess TGFβ activity in extracellular matrix (ECM) extracts, *C57Bl/6J* MEFs were plated in 6-well plates and treated for 20 min with 600 μg of ECM that was freshly extracted from Thbs1 Tg and littermate Ntg control quadriceps, as described below. For all experiments, cells were washed three times with ice-cold 1x PBS, collected, pelleted at 500×*g* at 4 °C, instantly frozen in liquid nitrogen and stored at −80 °C for further processing as described below.

In vivo* and *in vitro* adenoviral transduction—In vivo*, purified adenoviruses were injected into the left and right gastrocnemius muscles of 2-day-old Sprague-Dawley rat

pups (Harlan), followed by a second injection 72 h later ($3E10^8$ viral particles for each injection).[24] Rat pups were euthanized at 16 days of age. Tibia length was measured and gastrocnemius muscles were harvested, weighed, frozen in liquid nitrogen and stored −80°C until further use.

In vitro, NRVMs were isolated and plated in 10 cm gelatin coated culture dishes as described above.[22] Next, NRVMs infected with recombinant viruses to overexpress Thbs1, Thbs1Δt1 or βgal control for 3 h in serum free media, whereafter they were switched back to culture media (Hyclone Medium 19/Earle's Balanced Salt Solution (EBSS; ThermoScientific, SH20253FS) supplemented with 2% fetal bovine serum (Sigma Aldrich, Cat# F2442) and 1x penicillin-streptomycin (Corning Life Sciences, Cat# 30–0002-CI). Forty-eight hours later, cells were washed three times with sterile 1x PBS and switched to 5 mL serum-free media for 6 h whereafter both the media and NRVMs were collected for further analysis. The NRVMs were pelleted and processed for protein isolation as described below. The culture media was concentrated for protein (Amicon ultra-4 centrifugal filter devices, Millipore, Cat# UFC810024) to 250μL. FiveX SDS-PAGE loading buffer was added to 40 μL of the concentrated media and samples were analyzed by western blot as described below. In addition, InstantBlue® Coomassie protein stain was performed according to according to manufacturer's instructions (Abcam, Cat# ab119211) to visualize protein loading of the concentrated media.

MyoAAV production and injection in adult mice—Full length Thbs1 was obtained from the previously established pShuttle-CMV-Thbs1 vector,[22] amplified by PCR and cloned into the *SalI* and *HindIII* cloning sites of the pAAV-MCS vector (Cell biolabs, Cat# VPK-410) using the In-Fusion® HD cloning kit (Takara Bio; Cat# 639649).[22] The firefly luciferase cDNA was previously cloned into the pAAV-MCS vector (Cell biolabs, Cat# VPK-410).[26] Next, MyoAAV-Thbs1 and MyoAAV-Luciferase were produced in-house using the MyoAAV 1A capsid, and as previously described.[72–74] For example, recombinant virus was harvested from the HEK293 cells and media, and purified by ultracentrifuge using an iodixanol gradient.[73] AAV titers were determined by Taqman-based qPCR with C1000 Touch Thermal Cycler (Bio-Rad Laboratories). Next, 0.5E12 genomic copies of either MyoAAV-Thbs1 or MyoAAV-Luciferase control were delivered directly into the gastrocnemius muscle of 8-week-old *C57Bl/6J* mice. Six weeks later, mice were euthanized and the gastrocnemius muscle was excised to be snap frozen in liquid nitrogen and stored at stored −80°C until further use, or to be fixed overnight and embedded into O.C.T. (Tissue-Tek®, Sakura Finetek, Cat# 4583) as described below.

Forced treadmill running and grip strength—To assess muscle performance and endurance, mice were subjected to forced treadmill running and grip-strength measurements as previously described.[24,48] Briefly, mice were placed in individual lanes of a four-lane treadmill with 0–2.0 mA adjustable shock grid (Omni-Pacer LC4/M; Columbus Instruments International). A training regimen was established for 3 min with the shock grids deactivated, followed by 3 min with shock grids activated at a speed of 6 m/min to familiarize the mice with the environment. The speed was increased in increments of 2 m/min every 3 min to a maximum speed of 22 m/min. Exhaustion was determined as greater

than 10 consecutive seconds on the shock grid without attempting to re-engage running on the treadmill. Time spent on the treadmill before exhaustion or time to complete the protocol was recorded as average maximum time spent in exercise. The entire protocol was performed downhill (10% decline).

Forelimb grip strength (kg) of mice were measured using a Chatillon model DFIS-2 digital force transducer and normalized to body weight (kg) as previously described.[48] Each data point represents the average of 5 consecutive measurements per animal.

Histology—To assess overall tissue morphology, indicated muscles were harvested, weighed and fixed overnight in 4% paraformaldehyde (Electron Microscopy Sciences, Cat# 15714), dehydrated in 70% ethanol, and embedded in paraffin. Next, 5 μm thick transverse sections were obtained and stained with H&E and Masson's trichrome. For labeling with pSmad2/3, quadriceps tissue sections were rehydrated and heated in 1x antigen retrieval CITRA (BioGenex, Fremont, CA, Cat# HK086–9K). Muscle sections were permeabilized for 10 min in 0.3% Triton/PBS and then in a blocking buffer (0.1% Triton/PBS, 5% goat serum, 2% BSA) for 1 h at room temperature. Primary antibody incubations were overnight at 4°C (MaineHeatlh Institute for Research, Cat# D8591, dilution 1/50 in blocking buffer). Appropriate Alexa Fluor 488 (green) secondary antibody (Invitrogen, Waltham MA, 1:400 in blocking buffer) and wheat germ agglutinin, Alexa Fluor 594 conjugate (ThermoFisher, Cat# W11262 at 1:100) were applied in blocking buffer for 1 h at room temperature. Sections were mounted in ProLong™ Diamond Antifade Mountant with DAPI (Thermo Fisher, Cat# P36971) to stain nuclei and protect the staining from photo bleaching.

For all other fluorescent microscopy, freshly harvested tissue samples were fixed in 4% paraformaldehyde, washed 3 times with 1x PBS and cryoprotected in 30% sucrose/1x PBS overnight at 4°C before embedding in O.C.T. (Tissue-Tek®, Sakura Finetek, Cat# 4583). Next, 10 μm cryosections were collected, rinsed in 1x PBS, permeabilized for 10 min in 1x PBS with 0.3% Triton® X-100 (Sigma Aldrich, Cat# 8787) and then blocked for 30 min at room temperature in 1x PBS containing 5% normal goat or donkey serum (Jackson ImmunoResearch Laboratories, Cat# 005–000-121 or Cat# 017–000-121, respectively) and 0.1% Triton® X-100. Primary antibody incubations were performed overnight at 4°C for Thbs1 (R&D Systems, Cat# AF3074, 1:100 dilution), collagen type I (Abcam, Cat# ab34710, 1:300 dilution), laminin (Sigma Aldrich, Cat# L0663, dilution 1:200), GRP78/BiP (Sigma Aldrich, Cat# G8918, dilution 1:100), CD45 (BD Pharmingen, Cat# 553076, dilution 1/100) and embryonic myosin heavy chain (*Myh3*, Developmental Studies Hybridoma Bank, Cat# F1.652, 1:10 dilution) or a combination thereof. Then, Alexa Fluor 488 (green), Alexa Fluor 568 (red), or Alexa Fluor 647 secondary antibodies (Invitrogen, Waltham MA, 1:400) and/or wheat germ agglutinin conjugated to FITC (Lectin from Triticum vulgaris, Millipore Sigma, Cat# L4895 at 1:100) were applied in blocking buffer for 1 h at room temperature. Sections were mounted in ProLong™ Diamond Antifade Mountant with DAPI (Thermo Fisher, Cat# P36971) to stain nuclei and protect the staining from photo bleaching. All fluorescent imaging was performed under identical conditions using a Nikon A1+ confocal laser microscope system (Nikon Instruments) equipped with 40x H_2O objective (Nikon Instruments, NA = 1.15) and NIS Elements Advanced Research (AR) microscope imaging software (Nikon Instruments). Quantification of myofiber cell

surface area (CSA) was performed on at least 5 random pictures of WGA-stained muscles. A minimum of 500 muscle fibers were analyzed using ImageJ analysis software (National Institute of Health) per animal and per experiment.[75] Quantitative analysis of MyoAAV-Lucif. versus MyoAAV-Thbs1 positive (Pos.) and negative (Neg.) CSA was determined by Thbs1 and laminin staining on gastrocnemius sections at 14 weeks of age (see above).

Capillary counts were analyzed on cryosections, co-stained with biotinylated isolectin B4 (Vector Laboratories, #B-1205) and WGA-FITC (Lectin from Triticum vulgaris, Millipore Sigma, #L4895 at 1:100) for 1 h at room temperature, followed by treatment with streptavidin, Alexa 594 conjugate (ThermoFisher Scientific, #S11227 at 1:1000) for 1 h at room temperature to visualize isolectin B4. Sections were mounted in ProLong™ Diamond Antifade Mountant with DAPI (Thermo Fisher, Cat# P36971) to stain nuclei and protect the staining from photo bleaching. Pictures were taken with a Nikon A1 confocal microscope. Five random pictures at the quadriceps mid-belly were taken for quantitative analysis.

SUnSET and autophagic flux assay—To determine the rate of protein synthesis, a surface sensing of translation (SUnSET) assay was performed as previously described.[65] Briefly, mice were anesthetized and given an i.p. injection of 0.04 μM puromycin (in water; ThermoFisher, Cat# A113803) per gram of body weight or vehicle control. Exactly 30 minutes later, mice were euthanized and quadriceps was isolated, snap-frozen and stored −80°C until further use. To evaluate autophagic “flux”, mice were dosed i.p. with 0.4 mg per kg body weight per day colchicine (in water; Sigma Aldrich, Cat# C9754) for two days. At the same time, control mice received an equal volume of i.p. water, whereafter mice were euthanized, quadriceps was harvested, snap-frozen and stored −80°C until further use.[32] Next protein isolations and western blot analysis was performed as described below to assess the relative levels of puromycin-tagged proteins or levels of LC3b and p62 by western blot analysis as described below.

Protein isolation and western blotting—Protein isolations were obtained by homogenizing cells and tissues using a Fisherbrand™ 150 homogenizer (Fischer Scientific, Cat# 15–340-168) in ice-cold modified radio-immunoprecipitation assay (RIPA) buffer (1% Triton® X-100, 1% sodium deoxycholate, 0.1% sodium dodecyl sulfate (SDS), 50 mM Tris-HCl, pH 7.4, 150 mM NaCl) supplemented with Halt™ Protease and Phosphatase single-use inhibitor cocktail (Thermo Scientific, Cat# 78442). Samples were then sonicated (SP Scientific, Warminster, PA, VirSonic 60, power setting 3 for three times 10 s), cleared by centrifugation at 20,500 ×*g* for 14 min at 4 °C and stored at −80 °C until further use.

Sarcolemmal protein isolations were performed as previously described.[24] Briefly, quadriceps was harvested and homogenized in ice-cold lysis buffer (20 mM $Na_4P_2O_7$, 20 mM NaH_2PO_4, 1 mM $MgCl_2$, 0.303 M sucrose, 0.5 mM EDTA, pH 7.1 with Halt™ Protease and Phosphatase single-use inhibitor cocktail; Thermo Scientific, Cat# 78442), followed by centrifugation at 14,000 ×g for 20 min at 4°C. The supernatant was collected and the pellet was re-suspended, re-homogenized and re-centrifuged as described above. Finally, both supernatants were combined and the sarcolemmal fraction was pelleted at 30,000 ×g for 30 min at 4°C. This final pellet was then re-suspended in ice-cold RIPA buffer and stored at −80°C until further use.

ECM and microsomal extracts from quadriceps were generated using the Compartment Protein Extraction Kit following manufacturer's instructions (EMD Millipore, Cat# 2145). The final ECM pellet was solubilized in 8M urea dissolved in ammonium bicarbonate +10 mM DTT using a Biomasher II Closed System Micro Tissue Homogenizer (DWK Life Sciences Kimble™, Cat# 749625–0010).

Protein concentrations were determined using Direct Detect Spectrometer (Millipore Sigma, Cat# C134681) and Direct Detect® assay-free cards (Millipore Sigma, Cat# DDAC00010–8P). Protein concentrations of ECM fractions were determined using NanoDrop A280 measurements (DeNovix, Cat# DS-11 FX +). Equal amounts of protein were mixed with 5x Laemmli loading buffer, heated at 95 °C for 10 min and briefly centrifuged before loading on SDS-polyacrylamide gel electrophoresis (PAGE). A wet transfer method to Immobilon®-FL polyvinylidene fluoride (PVDF) membranes with a 0.45-μm pore size (Millipore, Cat# IPFL00010) was used, with exception of LC3b where proteins were transferred to Immobilon®-PSQ PVDF membranes with a 0.2-μm pore size (Millipore, Cat# ISEQ20200). Next, 5% blotto (nonfat dry milk [Carnation] in TBS with 0.2% Tween 20 [Fisher Scientific, Cat# BP337–500]) or phosphoBLOCKER™ blocking reagent (Cell Biolabs, Inc., Cat# AKR-104) was used to block membranes for 45 min at room temperature and to incubate the membranes in primary antibodies overnight at 4°C.

Immunoblots were performed using the primary antibodies listed below and visualized using an appropriate secondary antibody labeled with IRDye 800 and IRDye 680 (LI-COR Biosciences; all at 1:3000) in combination with an Odyssey CLx Infrared Imaging System (LI-COR). Staining of non-specific bands on PVDF membranes with Ponceau S solution (Sigma Aldrich, Cat# P7170) was used as a loading control for sarcolemmal isolates. In addition, InstantBlue® Coomassie protein stain was performed according to according to manufacturer's instructions (Abcam, Cat# ab119211) to visualize protein loading of the ECM fractions.

Primary antibodies used in this study were: Akt (Cell Signaling Technology, Cat# 9272 at 1:1000), p-Akt Ser473 (Cell Signaling Technology, Cat# 4060 at 1:1000), AMPKα (Cell Signaling Technology, Cat# 2532 at 1:1000), p-AMPKα Thr172 (Cell Signaling Technology, Cat# 2535 at 1:1000), ATF4 (Cell Signaling Technology, Cat# 11815 and LSBio LifeSpan Biosciences, Cat# LS-B6361; both at 1:1000), ATF6α (SAB SignalWayAntibody LLC, Cat# 24383; at 1:1000), BiP (Sigma, Cat# GG8918; at 1:1000), calreticulin (Cell Signaling Technology, Cat# 2891; at 1:1000), β-dystroglycan (developmental Studies Hybridoma Bank, cat# MANDAG2 clone 7D11; 1:100), p-4E-BP1 Thr37/46 (Cell Signaling Technology, Cat# 2855 at 1:1000), 4E-BP1 (Cell Signaling Technology, Cat# 9644 at 1:1000), FGF21 (R&D Systems, Cat# AF3057; at 1:500), Foxo1 (Cell Signaling Technology, Cat# 2880 at 1:1000), p-Foxo1 ser256 (Cell Signaling Technology, Cat# 9461 at 1:1000), Foxo3 (Cell Signaling Technology, Cat# 2497 at 1:1000), p-Foxo3 ser413 (Cell Signaling Technology, Cat# 8174 at 1:1000), p-Foxo3 ser 253 (Cell Signaling Technology, Cat# 9466 at 1:1000), IRE1α (Cell Signaling Technology, Cat# 3294; at 1:1000), β1D-integrin (Millipore, MAB1900; at 1:500), LAMP1 (Development Studies Hybridoma Bank, Cat# 1D4B; at 1:100), LAMP2 (Development Studies Hybridoma Bank, Cat# ABL-93; at 1:100), LC3b (Cell Signaling Technology, Cat# 3868; at 1:1000),

mTOR (Cell Signaling Technology, Cat# 2972 at 1:1000), *p*-mTOR ser2448 (Cell Signaling Technology, Cat# 2971 at 1:1000), p62 (Sigma, Cat# p0067 at 1:1000), LIMPII (Abcam, Cat# ab176317; at 1:1000), p-p70 S6K Thr389 (Cell Signaling Technology, Cat# 9205 at 1:1000), p70 S6K (Cell Signaling Technology, Cat# 2708 at 1:1000),PERK (Cell Signaling Technology, Cat# 3192; at 1:1000), anti-puromycin (Sigma, Cat# MABE343; at 1:1000); α-sarcoglycan (Development Studies Hybridoma Bank, Cat# IVD3(1)A9; at 1:100), β-sarcoglycan (Novus Biologicals, Cat# NBP1–90300; at 1:1000); δ-sarcoglycan (Abcam, Cat# ab137101; at 1:500); Smad2 (Cell Signaling Technology, Cat# 5339; at 1:1000); Smad3 (Abcam, Cat# ab40854; at 1:500); P-Smad2 Ser465/467/P-Smad3 Ser423/425 (Signaling Technology, Cat# 8828; at 1:1000); p-Smad3 Ser423/425 (Signaling Technology, Cat# 9520; at 1:1000); TGFβ RII (Santa Cruz Biotechnology, Cat# sc-17799; at 1:200); Thbs1 (R&D Systems, Cat# AF3074; at 1:500 and ThermoFisher Scientific, Cat# MA5–13395; at 1:1000); Thbs2 (R&D Systems, Cat# MAB1635; at 1:500); Thbs4 (R&D Systems, Cat# AF2390; at 1:500); Ubiquitin (Santa Cruz Biotechnology, Cat# sc-8017; at 1:200); and glyceraldehyde 3-phosphate dehydrogenase (Gapdh; Fitzgerald, Cat# 10R-G109A; at 1:10000) which served as overall loading control. All antibodies were authenticated for proper specificity, in some cases using tissues or cells from gene-deleted mice or using authentication data provided by the vendor for each antibody.

Transmission electron microscopy—Transmission electron microscopy was performed as previously described.[24] In short, quadriceps from anesthetized mice were harvested and immediately immersed in relaxing buffer (0.15% sucrose, 5% dextrose, 100 mM KCl in 1x PBS), fixed overnight (3.5% glutaraldehyde, 0.15% sucrose in 0.1 M sodium cacodylate ph 7.4), post-fixed for 2 h at room temperature in 1% OsO_4 (in water), washed, dehydrated and embedded using Epoxy resin (Electron Microscopy Sciences, Embed 812 Embedding Kit with BDMA, Cat# 14121). Next, ultrathin sections were generated and counterstained with 1.5% uranyl acetate, 70% ethanol and lead citrate. Images were obtained using a Hitachi 7600 transmission electron microscope connected to an AMT digital camera (AMT, Biosprint16).

Vesicular trafficking—Live cell quantitative imaging and photobleaching to evaluate ER-to-Golgi (FRAP) and Golgi-to-membrane vesicular trafficking (iFRAP) were performed in NRVMs as previously described.[24] In brief, NRVMs were infected with adenoviruses harboring Thbs1 or βgal 24 h prior to subjecting them to the protocols described below. For FRAP, NRVMs were then infected with a baculovirus encoding a red fluorescent protein (RFP)-tagged N-acetylgalactosaminyltransferase (GalNAcT2-RFP; CellLight™ Golgi-RFP Bacmam 2.0; Thermo Fisher, Cat# C10593), incubated overnight and then treated for 30 min with 100 μg/mL cycloheximide (Sigma-Aldrich, Cat# C4859) to block new protein synthesis. After acquiring a few baseline images, a region of interest (ROI) that encompasses the perinuclear Golgi network was bleached with a high intensity laser at 561 nm. RFP recovery was monitored and quantified for 2 h as a measure for ER-to-Golgi protein trafficking. For iFRAP, NRVMs were transduced with an adenovirus encoding a temperature-sensitive VSVG-eGFP fusion protein and incubated at 40°C for 24 h. The next day, cells were treated with cycloheximide for 1 h and incubated at 32°C to allow VSVG-eGFP to traffic from the ER to the Golgi apparatus. The Golgi cargo was selectively

highlighted by photobleaching the entire cell excluding the Golgi network using a high intensity laser at 488 nm, followed by time-lapse imaging for 2 h to monitor and quantify export of VSVG-eGFP from the Golgi apparatus as a measure of Golgi-to-plasma membrane trafficking. All live cell imaging was performed on a Nikon A1 confocal laser microscope system and equipped with Plan Apo 40x oil immersion objective (NA = 1.0), an INU-TIZ-F1 stage top incubator (Tokai hit CO, Ltd, Shizuoka-ken, Japan) and NIS Elements AR microscope imaging and analyses software (Nikon Instruments Inc.).

ELISA and proteasome activity assay—Levels of Thbs1 and endogenous TGFβ1 a were measured using an ELISA kit for Thbs1 (Uscn Life Science, Cat# SEA611Mu) or TGF-beta 1 Quantikine ELISA kit (R&D Systems, Cat# SMB100B), respectively. Chymotrypsin-like 20S proteasome activity in fresh quadriceps extracts was determined using the Proteasome Activity Assay Kit (Abcam, Cat# ab107921). All assays were performed following manufacturer's instructions.

QUANTIFICATION AND STATISTICAL ANALYSIS

All histological image analyses were performed using ImageJ. Immunoblots were analyzed using Image Studio Lite software from LI-COR. Live cell imaging data (FRAP and iFRAP) were analyzed using NIS Elements AR software (version 5.02) as previously described.[76]

All data are presented as mean ± standard error of mean (SEM). Statistical analyses were performed with GraphPad Prism 9 software. Details of all statistical tests used, *n*-values and what n represents are provided in the figure legends and on the histograms. When two experimental conditions or groups were being compared, we used an unpaired two-tailed t test. Comparison between more than two experimental conditions was performed using one-way analysis of variance (ANOVA) followed by Tukey's test for multiple comparison. Comparison of survival curves was performed using a two-tailed log rank (Mantel-Cox) test. For all tests, p-values < 0.05 was considered significant. p values from ANOVA are reported as multiplicity-adjusted p values. No data were excluded from any of the analyses.

Supplementary Material

Refer to Web version on PubMed Central for supplementary material.

ACKNOWLEDGMENTS

This work was supported by a grant from the National Heart, Lung, and Blood Institute of the NIH (R01HL105924 and R01HL162595) to J.D.M. The graphical abstract was created with BioRender (https://BioRender.com).

REFERENCES

1. Baskin KK, Winders BR, and Olson EN (2015). Muscle as a "mediator" of systemic metabolism. Cell Metabol. 21, 237–248. 10.1016/j.cmet.2014.12.021.
2. Sartori R, Romanello V, and Sandri M (2021). Mechanisms of muscle atrophy and hypertrophy: implications in health and disease. Nat. Commun. 12, 330. 10.1038/s41467-020-20123-1. [PubMed: 33436614]

3. Sandri M (2013). Protein breakdown in muscle wasting: role of autophagy-lysosome and ubiquitin-proteasome. Int. J. Biochem. Cell Biol. 45, 2121–2129. 10.1016/j.biocel.2013.04.023. [PubMed: 23665154]
4. Schiaffino S, Dyar KA, Ciciliot S, Blaauw B, and Sandri M (2013). Mechanisms regulating skeletal muscle growth and atrophy. FEBS J. 280, 4294–4314. 10.1111/febs.12253. [PubMed: 23517348]
5. Egerman MA, and Glass DJ (2014). Signaling pathways controlling skeletal muscle mass. Crit. Rev. Biochem. Mol. Biol. 49, 59–68. 10.3109/10409238.2013.857291. [PubMed: 24237131]
6. Zugmaier G, Paik S, Wilding G, Knabbe C, Bano M, Lupu R, Deschauer B, Simpson S, Dickson RB, and Lippman M (1991). Transforming growth factor beta 1 induces cachexia and systemic fibrosis without an antitumor effect in nude mice. Cancer Res. 51, 3590–3594. [PubMed: 2054795]
7. Sartori R, Milan G, Patron M, Mammucari C, Blaauw B, Abraham R, and Sandri M (2009). Smad2 and 3 transcription factors control muscle mass in adulthood. Am. J. Physiol. Cell Physiol. 296, C1248–C1257. 10.1152/ajpcell.00104.2009. [PubMed: 19357234]
8. Mendias CL, Gumucio JP, Davis ME, Bromley CW, Davis CS, and Brooks SV (2012). Transforming growth factor-beta induces skeletal muscle atrophy and fibrosis through the induction of atrogin-1 and scleraxis. Muscle Nerve 45, 55–59. 10.1002/mus.22232. [PubMed: 22190307]
9. Narola J, Pandey SN, Glick A, and Chen YW (2013). Conditional expression of TGF-beta1 in skeletal muscles causes endomysial fibrosis and myofibers atrophy. PLoS One 8, e79356. 10.1371/journal.pone.0079356. [PubMed: 24244485]
10. Tando T, Hirayama A, Furukawa M, Sato Y, Kobayashi T, Funayama A, Kanaji A, Hao W, Watanabe R, Morita M, et al. (2016). Smad2/3 Proteins Are Required for Immobilization-induced Skeletal Muscle Atrophy. J. Biol. Chem. 291, 12184–12194. 10.1074/jbc.M115.680579. [PubMed: 27129272]
11. Ábrigo J, Campos F, Simon F, Riedel C, Cabrera D, Vilos C, and Cabello-Verrugio C (2018). TGF-beta requires the activation of canonical and non-canonical signalling pathways to induce skeletal muscle atrophy. Biol. Chem. 399, 253–264. 10.1515/hsz-2017-0217. [PubMed: 29140787]
12. Egerman MA, Cadena SM, Gilbert JA, Meyer A, Nelson HN, Swalley SE, Mallozzi C, Jacobi C, Jennings LL, Clay I, et al. (2015). GDF11 Increases with Age and Inhibits Skeletal Muscle Regeneration. Cell Metabol. 22, 164–174. 10.1016/j.cmet.2015.05.010.
13. Kajabadi N, Low M, Jacques E, Lad H, Tung LW, Babaeijandaghi F, Gamu D, Zelada D, Wong CK, Chang C, et al. (2023). Activation of beta-catenin in mesenchymal progenitors leads to muscle mass loss. Dev. Cell 58, 489–505.e7. 10.1016/j.devcel.2023.02.009. [PubMed: 36898377]
14. Chen JL, Walton KL, Hagg A, Colgan TD, Johnson K, Qian H, Gregorevic P, and Harrison CA (2017). Specific targeting of TGF-beta family ligands demonstrates distinct roles in the regulation of muscle mass in health and disease. Proc. Natl. Acad. Sci. USA 114, E5266–E5275. 10.1073/pnas.1620013114. [PubMed: 28607086]
15. Gallot YS, and Bohnert KR (2021). Confounding Roles of ER Stress and the Unfolded Protein Response in Skeletal Muscle Atrophy. Int. J. Mol. Sci. 22, 2567. 10.3390/ijms22052567. [PubMed: 33806433]
16. Ebert SM, Monteys AM, Fox DK, Bongers KS, Shields BE, Malmberg SE, Davidson BL, Suneja M, and Adams CM (2010). The transcription factor ATF4 promotes skeletal myofiber atrophy during fasting. Mol. Endocrinol. 24, 790–799. 10.1210/me.2009-0345. [PubMed: 20197309]
17. Ebert SM, Dyle MC, Kunkel SD, Bullard SA, Bongers KS, Fox DK, Dierdorff JM, Foster ED, and Adams CM (2012). Stress-induced skeletal muscle Gadd45a expression reprograms myonuclei and causes muscle atrophy. J. Biol. Chem. 287, 27290–27301. 10.1074/jbc.M112.374777. [PubMed: 22692209]
18. Fox DK, Ebert SM, Bongers KS, Dyle MC, Bullard SA, Dierdorff JM, Kunkel SD, and Adams CM (2014). p53 and ATF4 mediate distinct and additive pathways to skeletal muscle atrophy during limb immobilization. Am. J. Physiol. Endocrinol. Metab. 307, E245–E261. 10.1152/ajpendo.00010.2014. [PubMed: 24895282]
19. Ebert SM, Bullard SA, Basisty N, Marcotte GR, Skopec ZP, Dierdorff JM, Al-Zougbi A, Tomcheck KC, DeLau AD, Rathmacher JA, et al. (2020). Activating transcription factor 4 (ATF4) promotes skeletal muscle atrophy by forming a heterodimer with the transcriptional regulator C/EBPbeta. J. Biol. Chem. 295, 2787–2803. 10.1074/jbc.RA119.012095. [PubMed: 31953319]

20. Miller MJ, Marcotte GR, Basisty N, Wehrfritz C, Ryan ZC, Strub MD, McKeen AT, Stern JI, Nath KA, Rasmussen BB, et al. (2023). The transcription regulator ATF4 is a mediator of skeletal muscle aging. Geroscience 45, 2525–2543. 10.1007/s11357-023-00772-y. [PubMed: 37014538]
21. Adams JC, and Lawler J (2011). The thrombospondins. Cold Spring Harbor Perspect. Biol. 3, a009712. 10.1101/cshperspect.a009712.
22. Lynch JM, Maillet M, Vanhoutte D, Schloemer A, Sargent MA, Blair NS, Lynch KA, Okada T, Aronow BJ, Osinska H, et al. (2012). A thrombospondin-dependent pathway for a protective ER stress response. Cell 149, 1257–1268. 10.1016/j.cell.2012.03.050. [PubMed: 22682248]
23. Brody MJ, Vanhoutte D, Schips TG, Boyer JG, Bakshi CV, Sargent MA, York AJ, and Molkentin JD (2018). Defective Flux of Thrombospondin-4 through the Secretory Pathway Impairs Cardiomyocyte Membrane Stability and Causes Cardiomyopathy. Mol. Cell Biol. 38, e00114–18. 10.1128/MCB.00114-18. [PubMed: 29712757]
24. Vanhoutte D, Schips TG, Kwong JQ, Davis J, Tjondrokoesoemo A, Brody MJ, Sargent MA, Kanisicak O, Yi H, Gao QQ, et al. (2016). Thrombospondin expression in myofibers stabilizes muscle membranes. Elife 5, e17589. 10.7554/eLife.17589. [PubMed: 27669143]
25. Schips TG, Vanhoutte D, Vo A, Correll RN, Brody MJ, Khalil H, Karch J, Tjondrokoesoemo A, Sargent MA, Maillet M, et al. (2019). Thrombospondin-3 augments injury-induced cardiomyopathy by intracellular integrin inhibition and sarcolemmal instability. Nat. Commun. 10, 76. 10.1038/s41467-018-08026-8. [PubMed: 30622267]
26. Vanhoutte D, Schips TG, Vo A, Grimes KM, Baldwin TA, Brody MJ, Accornero F, Sargent MA, and Molkentin JD (2021). Thbs1 induces lethal cardiac atrophy through PERK-ATF4 regulated autophagy. Nat. Commun. 12, 3928. 10.1038/s41467-021-24215-4. [PubMed: 34168130]
27. Stenina-Adognravi O (2014). Invoking the power of thrombospondins: regulation of thrombospondins expression. Matrix Biol. 37, 69–82. 10.1016/j.matbio.2014.02.001. [PubMed: 24582666]
28. Roudier E, Gineste C, Wazna A, Dehghan K, Desplanches D, and Birot O (2010). Angio-adaptation in unloaded skeletal muscle: new insights into an early and muscle type-specific dynamic process. J. Physiol. 588, 4579–4591. 10.1113/jphysiol.2010.193243. [PubMed: 20876198]
29. Tanaka M, Kanazashi M, Kondo H, and Fujino H (2022). Time course of capillary regression and an expression balance between vascular endothelial growth factor-A and thrombospondin-1 in the soleus muscle of hindlimb unloaded rats. Muscle Nerve 65, 350–360. 10.1002/mus.27478. [PubMed: 34957570]
30. Rong Z, Yang Z, Zhang C, Pu R, Chen C, Xu J, and Luo F (2023). Bioinformatics analysis of paravertebral muscles atrophy in adult degenerative scoliosis. J. Muscle Res. Cell Motil. 44, 287–297. 10.1007/s10974-023-09650-8. [PubMed: 37209232]
31. Gambara G, Salanova M, Ciciliot S, Furlan S, Gutsmann M, Schiffl G, Ungethuem U, Volpe P, Gunga HC, and Blottner D (2017). Gene Expression Profiling in Slow-Type Calf Soleus Muscle of 30 Days Space-Flown Mice. PLoS One 12, e0169314. 10.1371/journal.pone.0169314. [PubMed: 28076365]
32. Ju JS, Varadhachary AS, Miller SE, and Weihl CC (2010). Quantitation of “autophagic flux” in mature skeletal muscle. Autophagy 6, 929–935. 10.4161/auto.6.7.12785. [PubMed: 20657169]
33. Whitney ML, Jefferson LS, and Kimball SR (2009). ATF4 is necessary and sufficient for ER stress-induced upregulation of REDD1 expression. Biochem. Biophys. Res. Commun. 379, 451–455. 10.1016/j.bbrc.2008.12.079. [PubMed: 19114033]
34. Li Y, Li S, and Wu H (2022). Ubiquitination-Proteasome System (UPS) and Autophagy Two Main Protein Degradation Machineries in Response to Cell Stress. Cells 11, 851. 10.3390/cells11050851. [PubMed: 35269473]
35. Yoon MS (2017). mTOR as a Key Regulator in Maintaining Skeletal Muscle Mass. Front. Physiol. 8, 788. 10.3389/fphys.2017.00788. [PubMed: 29089899]
36. Bothe GW, Haspel JA, Smith CL, Wiener HH, and Burden SJ (2000). Selective expression of Cre recombinase in skeletal muscle fibers. Genesis 26, 165–166. [PubMed: 10686620]

37. Resovi A, Pinessi D, Chiorino G, and Taraboletti G (2014). Current understanding of the thrombospondin-1 interactome. Matrix Biol. 37, 83–91. 10.1016/j.matbio.2014.01.012. [PubMed: 24476925]

38. Pepino MY, Kuda O, Samovski D, and Abumrad NA (2014). Structure-function of CD36 and importance of fatty acid signal transduction in fat metabolism. Annu. Rev. Nutr. 34, 281–303. 10.1146/annurev-nutr-071812-161220. [PubMed: 24850384]

39. Yang H, Xun Y, and You H (2023). The landscape overview of CD47-based immunotherapy for hematological malignancies. Biomark. Res. 11, 15. 10.1186/s40364-023-00456-x. [PubMed: 36726125]

40. Bohnert KR, McMillan JD, and Kumar A (2018). Emerging roles of ER stress and unfolded protein response pathways in skeletal muscle health and disease. J. Cell. Physiol. 233, 67–78. 10.1002/jcp.25852. [PubMed: 28177127]

41. Crawford SE, Stellmach V, Murphy-Ullrich JE, Ribeiro SM, Lawler J, Hynes RO, Boivin GP, and Bouck N (1998). Thrombospondin-1 is a major activator of TGF-beta1 in vivo. Cell 93, 1159–1170. 10.1016/s0092-8674(00)81460-9. [PubMed: 9657149]

42. Murphy-Ullrich JE, and Suto MJ (2018). Thrombospondin-1 regulation of latent TGF-beta activation: A therapeutic target for fibrotic disease. Matrix Biol. 68–69, 28–43. 10.1016/j.matbio.2017.12.009. [PubMed: 29288716]

43. Ribeiro SM, Poczatek M, Schultz-Cherry S, Villain M, and Murphy-Ullrich JE (1999). The activation sequence of thrombospondin-1 interacts with the latency-associated peptide to regulate activation of latent transforming growth factor-beta. J. Biol. Chem. 274, 13586–13593. 10.1074/jbc.274.19.13586. [PubMed: 10224129]

44. Liu Z, Gu H, Gan L, Xu Y, Feng F, Saeed M, and Sun C (2017). Reducing Smad3/ATF4 was essential for Sirt1 inhibiting ER stress-induced apoptosis in mice brown adipose tissue. Oncotarget 8, 9267–9279. 10.18632/oncotarget.14035. [PubMed: 28030827]

45. González-González A, Muñoz-Muela E, Marchal JA, Cara FE, Molina MP, Cruz-Lozano M, Jiménez G, Verma A, Ramírez A, Qian W, et al. (2018). Activating Transcription Factor 4 Modulates TGFbeta-Induced Aggressiveness in Triple-Negative Breast Cancer via SMAD2/3/4 and mTORC2 Signaling. Clin. Cancer Res. 24, 5697–5709. 10.1158/1078-0432.CCR-17-3125. [PubMed: 30012564]

46. Daniel C, Wagner A, Hohenstein B, and Hugo C (2009). Thrombospondin-2 therapy ameliorates experimental glomerulonephritis via inhibition of cell proliferation, inflammation, and TGF-beta activation. Am. J. Physiol. Ren. Physiol. 297, F1299–F1309. 10.1152/ajprenal.00254.2009.

47. Schultz-Cherry S, Chen H, Mosher DF, Misenheimer TM, Krutzsch HC, Roberts DD, and Murphy-Ullrich JE (1995). Regulation of transforming growth factor-beta activation by discrete sequences of thrombospondin 1. J. Biol. Chem. 270, 7304–7310. 10.1074/jbc.270.13.7304. [PubMed: 7706271]

48. Accornero F, Kanisicak O, Tjondrokoesoemo A, Attia AC, McNally EM, and Molkentin JD (2014). Myofiber-specific inhibition of TGFbeta signaling protects skeletal muscle from injury and dystrophic disease in mice. Hum. Mol. Genet. 23, 6903–6915. 10.1093/hmg/ddu413. [PubMed: 25106553]

49. Ebert SM, Rasmussen BB, Judge AR, Judge SM, Larsson L, Wek RC, Anthony TG, Marcotte GR, Miller MJ, Yorek MA, et al. (2022). Biology of Activating Transcription Factor 4 (ATF4) and Its Role in Skeletal Muscle Atrophy. J. Nutr. 152, 926–938. 10.1093/jn/nxab440. [PubMed: 34958390]

50. Schultz-Cherry S, Lawler J, and Murphy-Ullrich JE (1994). The type 1 repeats of thrombospondin 1 activate latent transforming growth factor-beta. J. Biol. Chem. 269, 26783–26788. [PubMed: 7929414]

51. Young GD, and Murphy-Ullrich JE (2004). Molecular interactions that confer latency to transforming growth factor-beta. J. Biol. Chem. 279, 38032–38039. 10.1074/jbc.M405658200. [PubMed: 15208302]

52. Ebert SM, Dyle MC, Bullard SA, Dierdorff JM, Murry DJ, Fox DK, Bongers KS, Lira VA, Meyerholz DK, Talley JJ, and Adams CM (2015). Identification and Small Molecule Inhibition of an Activating Transcription Factor 4 (ATF4)-dependent Pathway to Age-related Skeletal Muscle

Weakness and Atrophy. J. Biol. Chem. 290, 25497–25511. 10.1074/jbc.M115.681445. [PubMed: 26338703]

53. Accornero F, van Berlo JH, Correll RN, Elrod JW, Sargent MA, York A, Rabinowitz JE, Leask A, and Molkentin JD (2015). Genetic Analysis of Connective Tissue Growth Factor as an Effector of Transforming Growth Factor beta Signaling and Cardiac Remodeling. Mol. Cell Biol. 35, 2154–2164. 10.1128/MCB.00199-15. [PubMed: 25870108]
54. Koitabashi N, Danner T, Zaiman AL, Pinto YM, Rowell J, Mankowski J, Zhang D, Nakamura T, Takimoto E, and Kass DA (2011). Pivotal role of cardiomyocyte TGF-beta signaling in the murine pathological response to sustained pressure overload. J. Clin. Invest. 121, 2301–2312. 10.1172/JCI44824. [PubMed: 21537080]
55. Vainshtein A, and Sandri M (2020). Signaling Pathways That Control Muscle Mass. Int. J. Mol. Sci. 21, 4759. 10.3390/ijms21134759. [PubMed: 32635462]
56. Grumati P, Coletto L, Sabatelli P, Cescon M, Angelin A, Bertaggia E, Blaauw B, Urciuolo A, Tiepolo T, Merlini L, et al. (2010). Autophagy is defective in collagen VI muscular dystrophies, and its reactivation rescues myofiber degeneration. Nat. Med. 16, 1313–1320. 10.1038/nm.2247. [PubMed: 21037586]
57. Xia Q, Huang X, Huang J, Zheng Y, March ME, Li J, and Wei Y (2021). The Role of Autophagy in Skeletal Muscle Diseases. Front. Physiol. 12, 638983. 10.3389/fphys.2021.638983. [PubMed: 33841177]
58. Masiero E, Agatea L, Mammucari C, Blaauw B, Loro E, Komatsu M, Metzger D, Reggiani C, Schiaffino S, and Sandri M (2009). Autophagy is required to maintain muscle mass. Cell Metabol. 10, 507–515. 10.1016/j.cmet.2009.10.008.
59. Raben N, Hill V, Shea L, Takikita S, Baum R, Mizushima N, Ralston E, and Plotz P (2008). Suppression of autophagy in skeletal muscle uncovers the accumulation of ubiquitinated proteins and their potential role in muscle damage in Pompe disease. Hum. Mol. Genet. 17, 3897–3908. 10.1093/hmg/ddn292. [PubMed: 18782848]
60. Kiyono K, Suzuki HI, Matsuyama H, Morishita Y, Komuro A, Kano MR, Sugimoto K, and Miyazono K (2009). Autophagy is activated by TGF-beta and potentiates TGF-beta-mediated growth inhibition in human hepatocellular carcinoma cells. Cancer Res. 69, 8844–8852. 10.1158/0008-5472.CAN-08-4401. [PubMed: 19903843]
61. B'Chir W, Maurin AC, Carraro V, Averous J, Jousse C, Muranishi Y, Parry L, Stepien G, Fafournoux P, and Bruhat A (2013). The eIF2alpha/ATF4 pathway is essential for stress-induced autophagy gene expression. Nucleic Acids Res. 41, 7683–7699. 10.1093/nar/gkt563. [PubMed: 23804767]
62. Rashid HO, Yadav RK, Kim HR, and Chae HJ (2015). ER stress: Autophagy induction, inhibition and selection. Autophagy 11, 1956–1977. 10.1080/15548627.2015.1091141. [PubMed: 26389781]
63. Crombie R, and Silverstein R (1998). Lysosomal integral membrane protein II binds thrombospondin-1. Structure-function homology with the cell adhesion molecule CD36 defines a conserved recognition motif. J. Biol. Chem. 273, 4855–4863. 10.1074/jbc.273.9.4855. [PubMed: 9478926]
64. Park BV, Freeman ZT, Ghasemzadeh A, Chattergoon MA, Rutebemberwa A, Steigner J, Winter ME, Huynh TV, Sebald SM, Lee SJ, et al. (2016). TGFbeta1-Mediated SMAD3 Enhances PD-1 Expression on Antigen-Specific T Cells in Cancer. Cancer Discov. 6, 1366–1381. 10.1158/2159-8290.CD-15-1347. [PubMed: 27683557]
65. Hindi SM, Sato S, Xiong G, Bohnert KR, Gibb AA, Gallot YS, McMillan JD, Hill BG, Uchida S, and Kumar A (2018). TAK1 regulates skeletal muscle mass and mitochondrial function. JCI Insight 3, e98441. 10.1172/jci.insight.98441. [PubMed: 29415881]
66. Durkin ME, Qian X, Popescu NC, and Lowy DR (2013). Isolation of Mouse Embryo Fibroblasts. Bio. Protoc. 3, e908. 10.21769/bioprotoc.908.
67. Khalil H, Kanisicak O, Prasad V, Correll RN, Fu X, Schips T, Vagnozzi RJ, Liu R, Huynh T, Lee SJ, et al. (2017). Fibroblast-specific TGF-beta-Smad2/3 signaling underlies cardiac fibrosis. J. Clin. Invest. 127, 3770–3783. 10.1172/JCI94753. [PubMed: 28891814]
68. Corbett MA, Robinson CS, Dunglison GF, Yang N, Joya JE, Stewart AW, Schnell C, Gunning PW, North KN, and Hardeman EC (2001). A mutation in alpha-tropomyosin(slow) affects muscle

strength, maturation and hypertrophy in a mouse model for nemaline myopathy. Hum. Mol. Genet. 10, 317–328. 10.1093/hmg/10.4.317. [PubMed: 11157795]

69. Yamamoto K, Sato T, Matsui T, Sato M, Okada T, Yoshida H, Harada A, and Mori K (2007). Transcriptional induction of mammalian ER quality control proteins is mediated by single or combined action of ATF6alpha and XBP1. Dev. Cell 13, 365–376. 10.1016/j.devcel.2007.07.018. [PubMed: 17765680]
70. Hack AA, Lam MY, Cordier L, Shoturma DI, Ly CT, Hadhazy MA, Hadhazy MR, Sweeney HL, and McNally EM (2000). Differential requirement for individual sarcoglycans and dystrophin in the assembly and function of the dystrophin-glycoprotein complex. J. Cell Sci. 113, 2535–2544. 10.1242/jcs.113.14.2535. [PubMed: 10862711]
71. Anders S, and Huber W (2010). Differential expression analysis for sequence count data. Genome Biol. 11, R106. 10.1186/gb-2010-11-10-r106. [PubMed: 20979621]
72. Tabebordbar M, Lagerborg KA, Stanton A, King EM, Ye S, Tellez L, Krunnfusz A, Tavakoli S, Widrick JJ, Messemer KA, et al. (2021). Directed evolution of a family of AAV capsid variants enabling potent muscle-directed gene delivery across species. Cell 184, 4919–4938.e22. 10.1016/j.cell.2021.08.028. [PubMed: 34506722]
73. Challis RC, Ravindra Kumar S, Chan KY, Challis C, Beadle K, Jang MJ, Kim HM, Rajendran PS, Tompkins JD, Shivkumar K, et al. (2019). Systemic AAV vectors for widespread and targeted gene delivery in rodents. Nat. Protoc. 14, 379–414. 10.1038/s41596-018-0097-3. [PubMed: 30626963]
74. Huo J, Prasad V, Grimes KM, Vanhoutte D, Blair NS, Lin SC, Bround MJ, Bers DM, and Molkentin JD (2023). MCUb is an inducible regulator of calcium-dependent mitochondrial metabolism and substrate utilization in muscle. Cell Rep. 42, 113465. 10.1016/j.celrep.2023.113465. [PubMed: 37976157]
75. Schneider CA, Rasband WS, and Eliceiri KW (2012). NIH Image to ImageJ: 25 years of image analysis. Nat. Methods 9, 671–675. 10.1038/nmeth.2089. [PubMed: 22930834]
76. Patterson GH, Hirschberg K, Polishchuk RS, Gerlich D, Phair RD, and Lippincott-Schwartz J (2008). Transport through the Golgi apparatus by rapid partitioning within a two-phase membrane system. Cell 133, 1055–1067. 10.1016/j.cell.2008.04.044. [PubMed: 18555781]

Highlights

- Thbs1 expression is induced in skeletal muscle under conditions causing atrophy
- Thbs1 overexpression induces profound skeletal muscle atrophy
- Thbs1-induced skeletal muscle atrophy is through TGFβ-Smad2/3 signaling
- Thbs1-null mice are resistant to denervation- and starvation-induced muscle atrophy

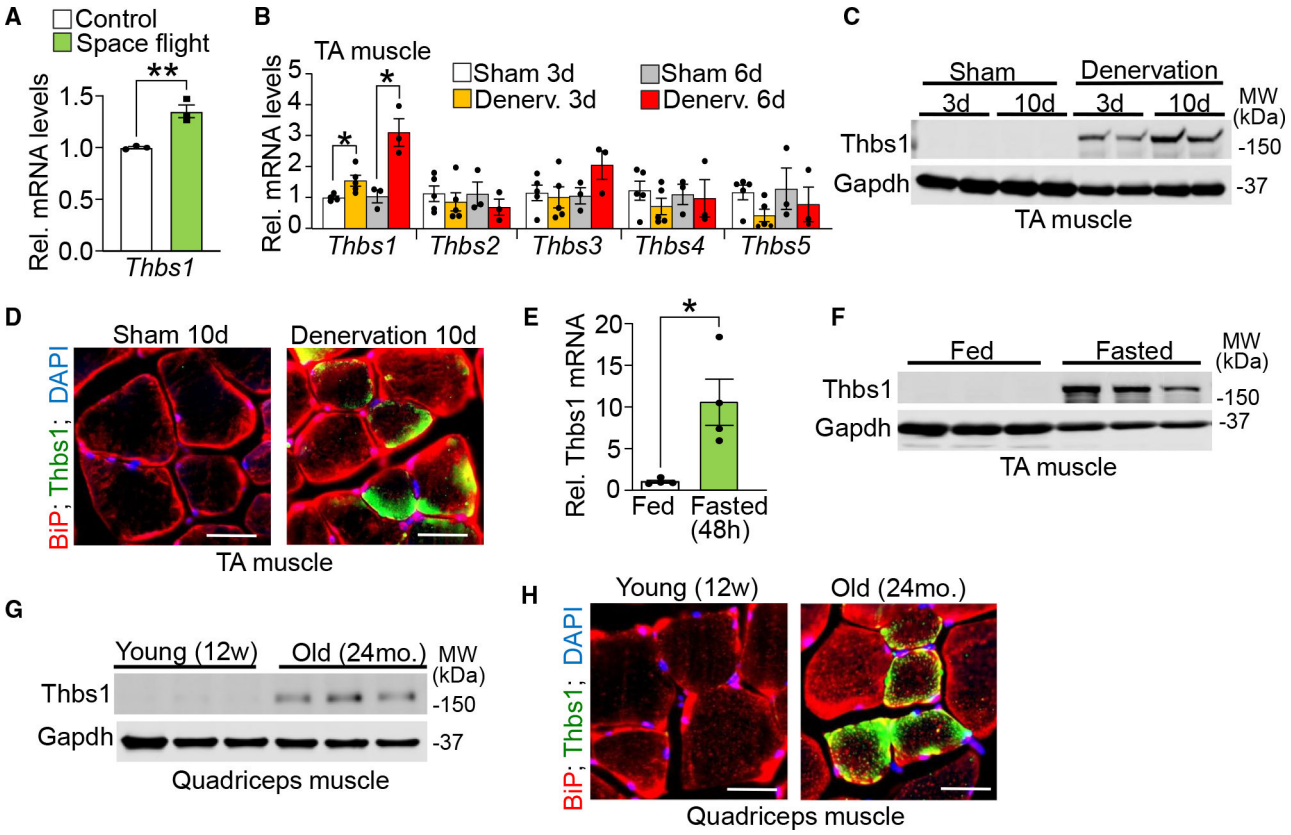

Figure 1. Thbs1 is induced in mouse models of skeletal muscle atrophy

(A) Fold change in the expression of *Thbs1* mRNA in soleus following 30 days of microgravity exposure (space flight) compared to control. Microarray dataset GEO: GSE80223 was analyzed from the Gene Expression Omnibus repository.[31] Error bars denote ±SEM from $n = 3$ biologically independent animals per group; $^{**}p < 0.01$ by two-tailed unpaired Student's t test.

(B) RT-qPCR for *Thbs1*, *Thbs2*, *Thbs3*, *Thbs4*, and *Thbs5* mRNA in the right tibialis anterior (TA) of 12-week-old wild-type (WT) mice subjected to 3 or 6 days (d) of unilateral hindlimb denervation, compared contralateral sham-operated leg. Error denote ±SEM from $n = 3$–5 biologically independent animals per group. $^{*}p < 0.05$ by two-tailed unpaired Student's t test.

(C) Western blot for Thbs1 and Gapdh control in right TA of 12-week-old WT mice subjected to 3 or 10 days (d) of unilateral hindlimb denervation, compared to contralateral, sham-operated TA. $n = 2$ biologically independent animals per time point.

(D) Representative immunohistochemistry for endogenous Thbs1 (green) and BiP (red) to visualize the endoplasmic reticulum (ER) on cryo-embedded TA of WT mice subjected to 10 days (d) of denervation compared to sham-operated controls at 12 weeks of age. Nuclei are shown in blue with DAPI. Scale bars represent 50 μm.

(E) RT-qPCR for *Thbs1* mRNA from TA of 8-week-old mice fed *ad libitum* or fasted for 48 h. Data are presented as fold expression over fed WT; error bars denote ±SEM from $n = 4$ biologically independent animals analyzed per group. $^{*}p < 0.05$ by two-tailed unpaired Student's t test.

(F and G) Western blot for Thbs1 and Gapdh in TA of 8-week-old mice fed *ad libitum* or fasted for 48 h (F), and in young (12 weeks of age) and old (24 months of age) WT quadriceps (G).

(H) Representative immunohistochemistry for endogenous Thbs1 (green), BiP (red), and the nucleus (DAPI, blue) on cryo-embedded 12-week-old (“young”) and 24-month-old (“old”) WT quadriceps. Scale bars represent 50 μm.

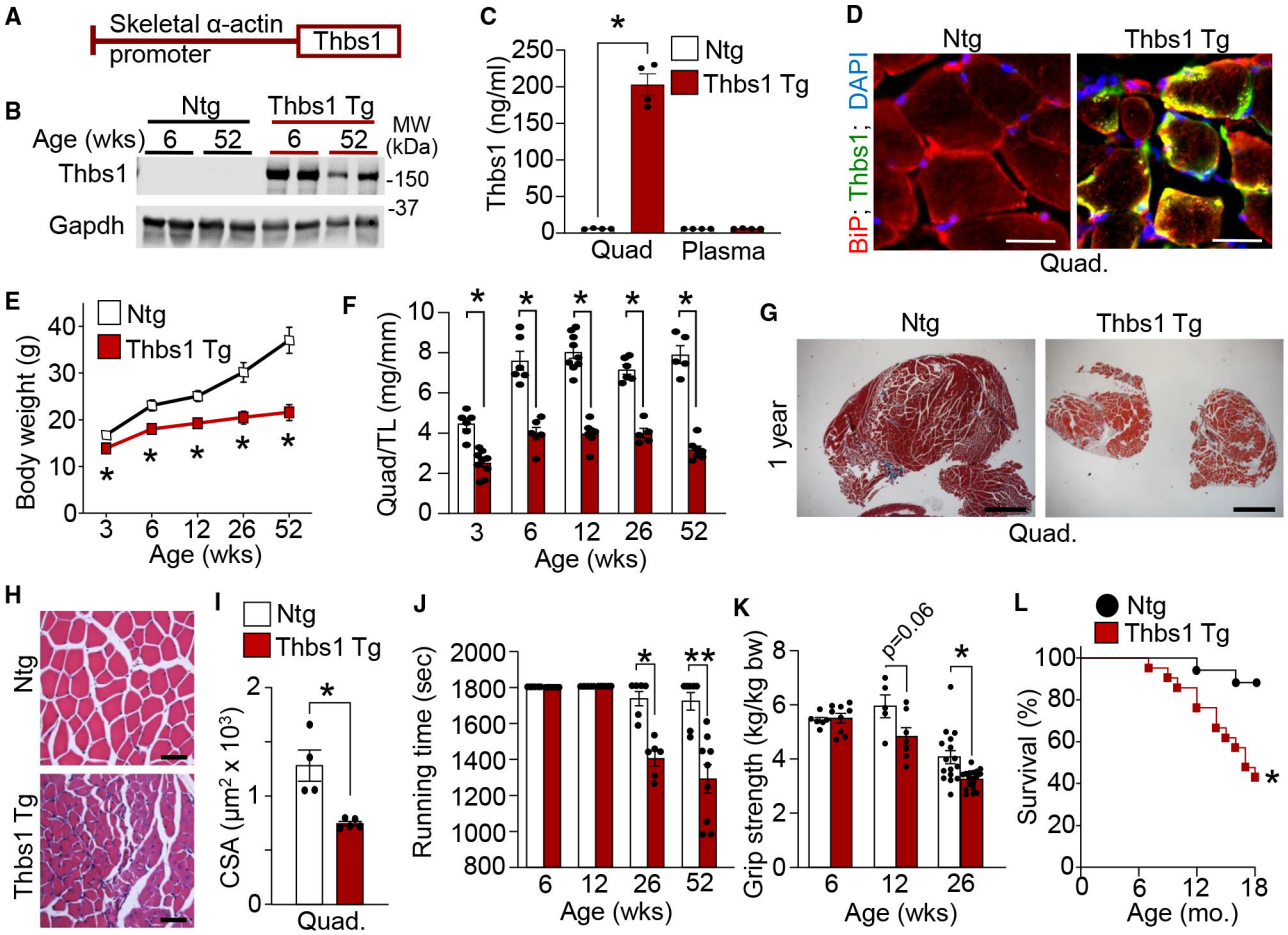

Figure 2. Transgene-mediated overexpression of Thbs1 induces skeletal muscle atrophy

(A) Schematic diagram of the Thbs1 skeletal muscle-specific transgene.

(B) Western blot analyses for Thbs1 or Gapdh control from quadriceps from non-transgenic (Ntg) and skeletal muscle-specific Thbs1 transgenic (Tg) mice at 6 and 52 weeks of age (n = 2 biological replicates per genotype and per time point).

(C) Thbs1 protein levels (ng/mL) determined by ELISA in quadriceps (Quad) and plasma obtained from Ntg and Thbs1 Tg mice at 6 weeks of age. Error bars denote ±SEM from n = 4 biologically independent animals per genotype. *p < 0.0001 by two-tailed unpaired Student's t test).

(D) Immunohistochemical fluorescent labeling of Thbs1 (green) and BiP to show the ER (red) on cryo-embedded quadriceps (Quad.) from Ntg and Thbs1 Tg mice at 6 weeks of age. Nuclei are visualized in blue (DAPI). Representative images of four mice per genotype are shown. Scale bars represent 50 μm.

(E and F) Body weight (E) and quadriceps (Quad) weight normalized to tibia length (F) of Ntg and Thbs1 Tg mice at the indicated ages in weeks (wks). Error bars denote ±SEM from n = 5–9 biologically independent animals per genotype and per age. *p < 0.001 (E) and *p < 0.0001 (F) by two-tailed unpaired Student's t test).

(G) Representative Masson's trichrome-stained histological sections of Ntg and Thbs1 Tg quadriceps (Quad) at 1 year of age. Representative images of five mice per genotype are shown. Scale bar represents 1 mm.
(H) H&E histological staining on quadriceps sections from Ntg and Thbs1 Tg at 6 weeks of age. Representative images of 4–5 mice per genotype are shown. Scale bars represent 50 μm.
(I) Myofiber cross-sectional area (CSA) in quadriceps (Quad) from Ntg and Thbs1 Tg mice at 6 weeks of age (n = 4–5 biologically independent animals per genotype; *p < 0.01 by two-tailed unpaired Student's t test). The legend above the bar plot also applies to (J) and (K).
(J and K) Running time to fatigue in seconds (sec) with a forced downhill treadmill (J) and forelimb grip strength (kg/kg body weight; K) from Ntg and Thbs1 Tg mice at the indicated ages in weeks (n = 5–18 biologically independent animals per genotype and per indicated age; *p < 0.01 and **p < 0.001 by two-tailed unpaired Student's t test).
(L) Kaplan-Meier survival plot of Ntg (n = 17) and Thbs1 Tg (n = 21) mice at the indicated ages. *p < 0.01, analyzed by two-tailed log-rank test.
See also Figures S1 and S2.

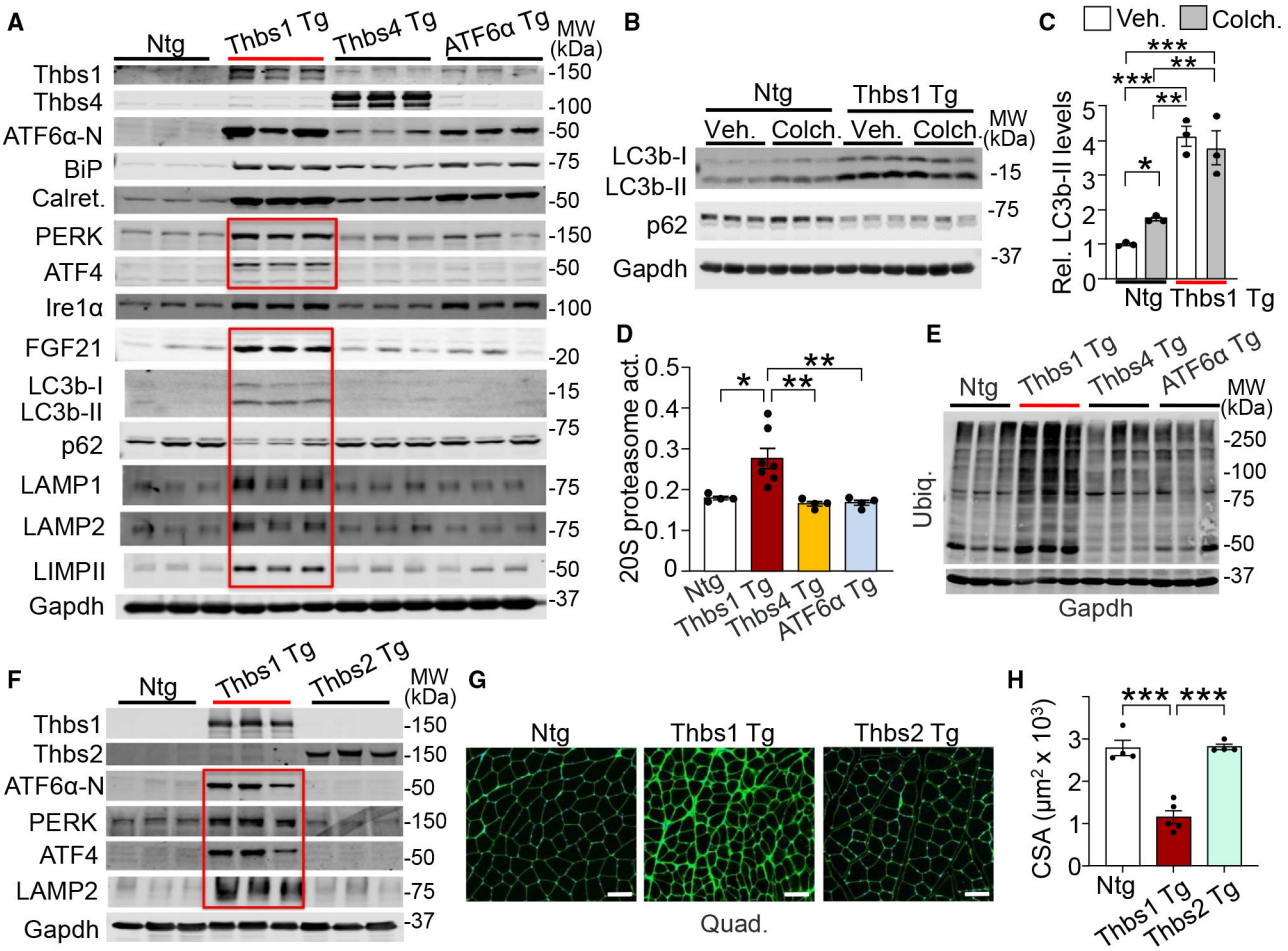

Figure 3. Thbs1 induces PERK, ATF4, and protein degradation in skeletal muscle

(A) Representative western blots for Thbs1, Thbs4, ATF6α-N (50 kDa, nuclear), BiP, calreticulin (Calret.), PERK, ATF4, IRE1α, fibroblast growth factor 21 (FGF21), LC3b, p62, LAMP1, LAMP2, and LIMPII from quadriceps protein extracts from Ntg and skeletal muscle-specific Thbs1 Tg, Thbs4 Tg, and ATF6α Tg mice at 6 weeks of age. Gapdh serves as a processing and loading control; $n = 3$ biologically independent animals per genotype. Red boxed areas show specific expression changes in Thbs1 Tg muscle.

(B and C) Representative western blots for LC3b, p62, and Gapdh as a loading control in 6-week-old quadriceps protein extracts from Ntg and Thbs1 Tg mice treated with water as vehicle (Veh.) or 0.4 mg/kg/day colchicine (Colch.) for 2 days to impact autolysosome content/activity. (C) Quantitative analysis of LC3b-II protein levels relative to Gapdh from the experiment shown in (B). Error bars denote ±SEM from $n = 3$ biologically independent animals per genotype and per treatment. *$p < 0.05$, **$p < 0.01$, ***$p < 0.001$ by one-way ANOVA and Tukey's multiple comparison test.

(D) 20S chymotrypsin-like proteasome activity (pmol/[min·μg]) in quadriceps tissue of Ntg and skeletal muscle-specific Thbs1 Tg, Thbs4 Tg, and ATF6α Tg mice at 6 weeks of age. Error bars denote ±SEM from $n = 4$–7 biologically independent animals per indicated genotype. *$p < 0.05$, **$p < 0.001$ by one-way ANOVA and Tukey's multiple comparison test.

(E) Representative western blot for ubiquitin-conjugated proteins (Ubiq.) in quadriceps tissue of the indicated genotypes of mice at 6 weeks of age. Gapdh serves as loading control; $n = 3$ biologically independent animals per genotype. Quantitative analysis of this experiment is presented in Figure S4A.

(F) Representative western blots for Thbs1, Thbs2, ATF6α-N (50 kDa, nuclear), PERK, ATF4, and LAMP2 from quadriceps protein extracts from Ntg and skeletal muscle-specific Thbs1 Tg and Thbs2 Tg mice at 12 weeks of age. Gapdh serves as loading control; $n = 3$ biologically independent animals per genotype.

(G) Immunohistochemistry micrographs showing wheat germ agglutinin (WGA, green) and DAPI (blue) in quadriceps of Ntg, Thbs1 Tg, and Thbs2 Tg at 12 weeks of age. Scale bars represent 100 μm.

(H) Myofiber cross-sectional area (CSA) in Ntg, Thbs1 Tg, and Thbs2 Tg quadriceps at 12 weeks of age as shown in (G). Error bars denote ±SEM from $n = 4–5$ biologically independent animals per genotype. ***$p < 0.001$ by one-way ANOVA and Tukey's multiple comparison test.

See also Figures S3 and S4.

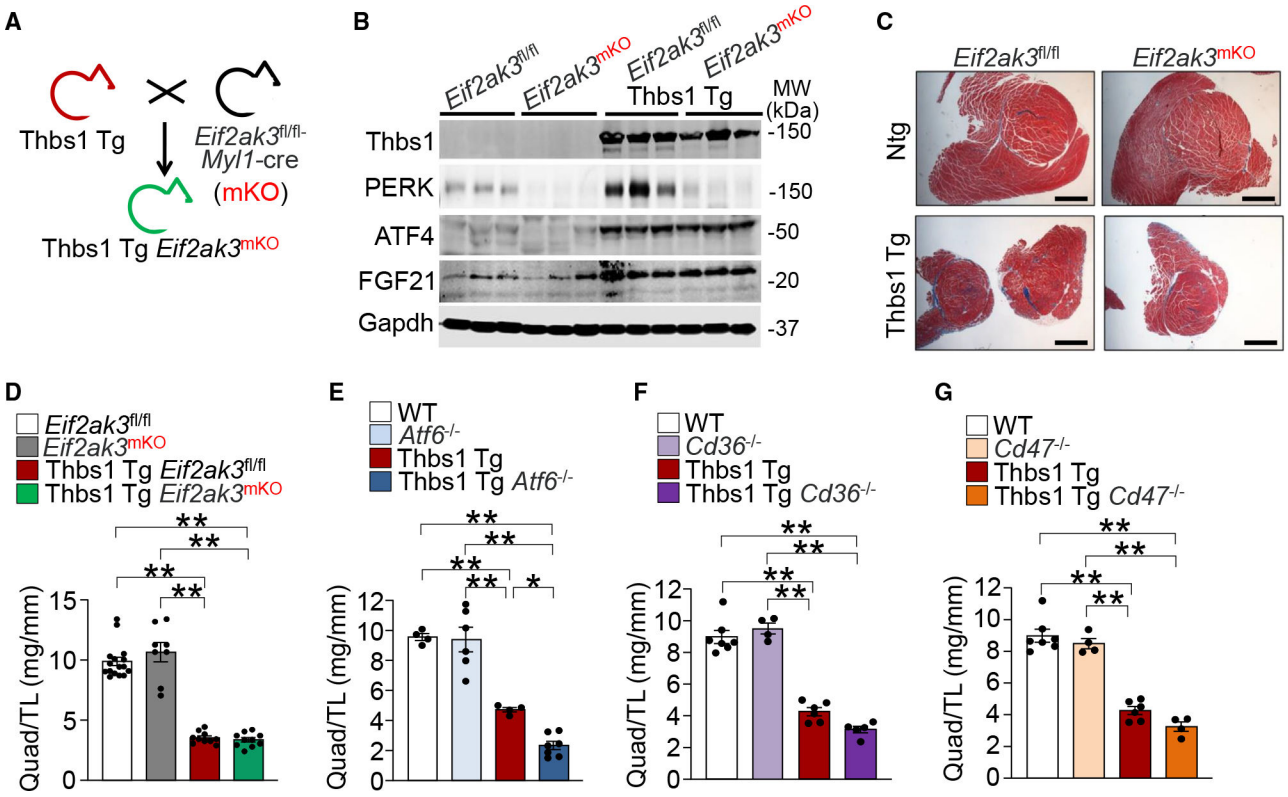

Figure 4. Loss of *Eif2ak3* (PERK), *Atf6*, *Cd36*, or *Cd47* does not rescue Thbs1-mediated skeletal muscle atrophy

(A) Breeding scheme to generate muscle-specific deletion of *Eif2ak3* (PERK; referred to as *Eif2ak3*^{mKO}) in Thbs1 Tg mice using *Eif2ak3*-LoxP-targeted (*Eif2ak3*$^{fl/fl}$) mice crossed with *Myl1*-cre gene-targeted mice.

(B) Western blots for Thbs1, PERK, ATF4, and FGF21 from quadriceps protein extracts from *Eif2ak3*$^{fl/fl}$, *Eif2ak3*^{mKO}, Thbs1 Tg *Eif2ak3*$^{fl/fl}$, and Thbs1 Tg *Eif2ak3*^{mKO} mice at 12 weeks of age. Gapdh serves as loading control; $n = 3$ biologically independent animals per genotype.

(C) Representative Masson's trichrome-stained histological sections of quadriceps from the indicated genotypes at 12 weeks of age. Representative images of six mice per genotype are shown. Scale bars represent 1 mm.

(D–G) Quadriceps (Quad) weight normalized to tibia length of (D) *Eif2ak3*$^{fl/fl}$, *Eif2ak3*^{mKO}, Thbs1 Tg *Eif2ak3*$^{fl/fl}$, and Thbs1 Tg *Eif2ak3*^{mKO} mice, (E) wild-type (WT), *Atf6*$^{-/-}$, Thbs1 Tg, and Thbs1 Tg *Atf6*$^{-/-}$ mice, (F) WT, *Cd36*$^{-/-}$, Thbs1 Tg, and Thbs1 Tg *Cd36*$^{-/-}$ mice, and (G) WT, *Cd47*$^{-/-}$, Thbs1 Tg, and Thbs1 Tg *Cd47*$^{-/-}$ mice at 12 weeks of age for (D), (F), and (G) and 8 weeks of age for (E). Error bars denote ±SEM. *$p < 0.05$, **$p < 0.0001$ by one-way ANOVA and Tukey's multiple comparison test.

See also Figure S5.

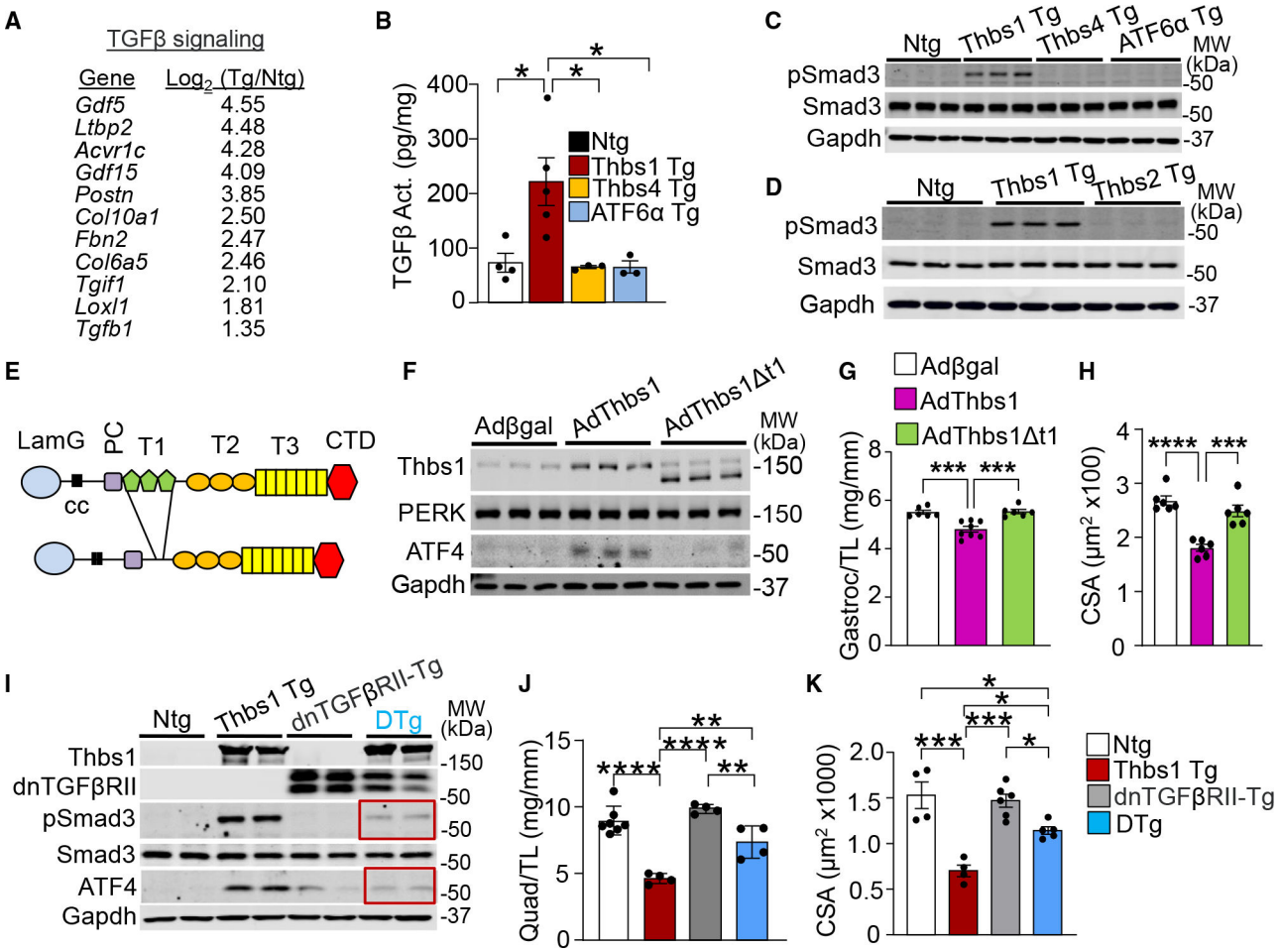

Figure 5. Thbs1 activates TGFβ-Smad3-ATF4 signaling to facilitate skeletal muscle atrophy

(A) Log_2 fold changes of mRNA expression in TGFβ signaling-associated genes between 6-week-old Thbs1 Tg and Ntg control quadriceps assessed by RNA sequencing. Full RNA-sequencing data were deposited in the GEO (GEO: GSE245663). *Gdf5*, growth differentiation factor 5; *Ltbp2*, latent transforming growth factor β binding protein 2; *Acvr1c*, activating receptor type 1C; *Gdf15*, growth differentiation factor 15; *Postn*, periostin; *Col10a1*, collagen type 10 alpha 1; *Fbn2*, fibrillin 2, *Col6a5*, collagen type 6 alpha 5; *Tgif1*, TGFβ-induced factor homeobox 1; *Loxl1*, lysyl oxidase-like 1; *Tgfb1*, transforming growth factor β1.

(B) Endogenous TGFβ activity levels in quadriceps protein extracts from Ntg, Thbs1 Tg, Thbs4 Tg, and ATF6α Tg mice at 6 weeks of age. Error bars denote ±SEM. *$p < 0.05$ by one-way ANOVA and Tukey's multiple comparison test.

(C and D) Representative western blots for phospho-Smad3 (Ser423/425) and total Smad3 in 6-week-old quadriceps protein extracts from the indicated skeletal muscle-specific transgenic mice. Gapdh serves as loading control; $n = 3$ biologically independent animals per genotype.

(E) Schematic diagram of wild-type Thbs1 domain structure and the Thbs1Δt1 mutant lacking the type-1 repeat domain. Each wild-type Thbs1 monomer consists of an N-terminal

laminin G (LamG) domain, a coiled-coil domain (cc), a procollagen homology domain (PC), type-1, −2, and −3 repeats (T1, T2 and T3), and a carboxy-terminal domain (CTD).
(F) Representative western blot analysis for Thbs1, PERK, and ATF4 in gastrocnemius protein extracts from 16-day-old rat pups injected with Adβgal, AdThbs1, or AdThbs1Δt1 mutant on postnatal day 2, followed by a second “boost” injection 72 h later (3E8 viral particles per injection). Gapdh serves as loading control; $n = 3$ biologically independent animals per genotype.
(G and H) Gastrocnemius (Gastroc) weight normalized to tibia length (TL; G) and myofiber cross-sectional area (CSA; H) from 16-day-old rat pups injected with Adβgal, AdThbs1, or AdThbs1Δt1 mutant following the timeline described for (F) (all 3E8 viral particles per injection). Error bars denote ±SEM from $n = 6–8$ biologically independent animals per treatment group. ***$p < 0.001$, ****$p < 0.0001$ by one-way ANOVA and Tukey’s multiple comparison test.
(I) Western blots for Thbs1, dominant-negative TGFβ type II receptor (dnTGFβRII), phospho-Smad3 (Ser423/425), total Smad3, ATF4, and Gapdh control in 12-week-old quadriceps obtained from Ntg, Thbs1 Tg, skeletal muscle-specific Tg mice expressing dnTGFβRII (dnTGFβRII Tg), and Thbs1-dnTGFβRII double Tg (DTg) mice. $n = 2$ biologically independent animals per genotype.
(J and K) Quadriceps (Quad) weight normalized to tibia length (J) and myofiber cross-sectional area (CSA; K) in Ntg, Thbs1 Tg, dnTGFβRII Tg, and Thbs1-dnTGFβRII double Tg (DTg) mice at 3 months of age. Error bars denote ±SEM from $n = 4–7$ biologically independent animals per genotype. *$p < 0.05$, **$p < 0.01$, ***$p < 0.001$, ****$p < 0.0001$ by one-way ANOVA and Tukey’s multiple comparison test.
See also Figures S6 and S7.

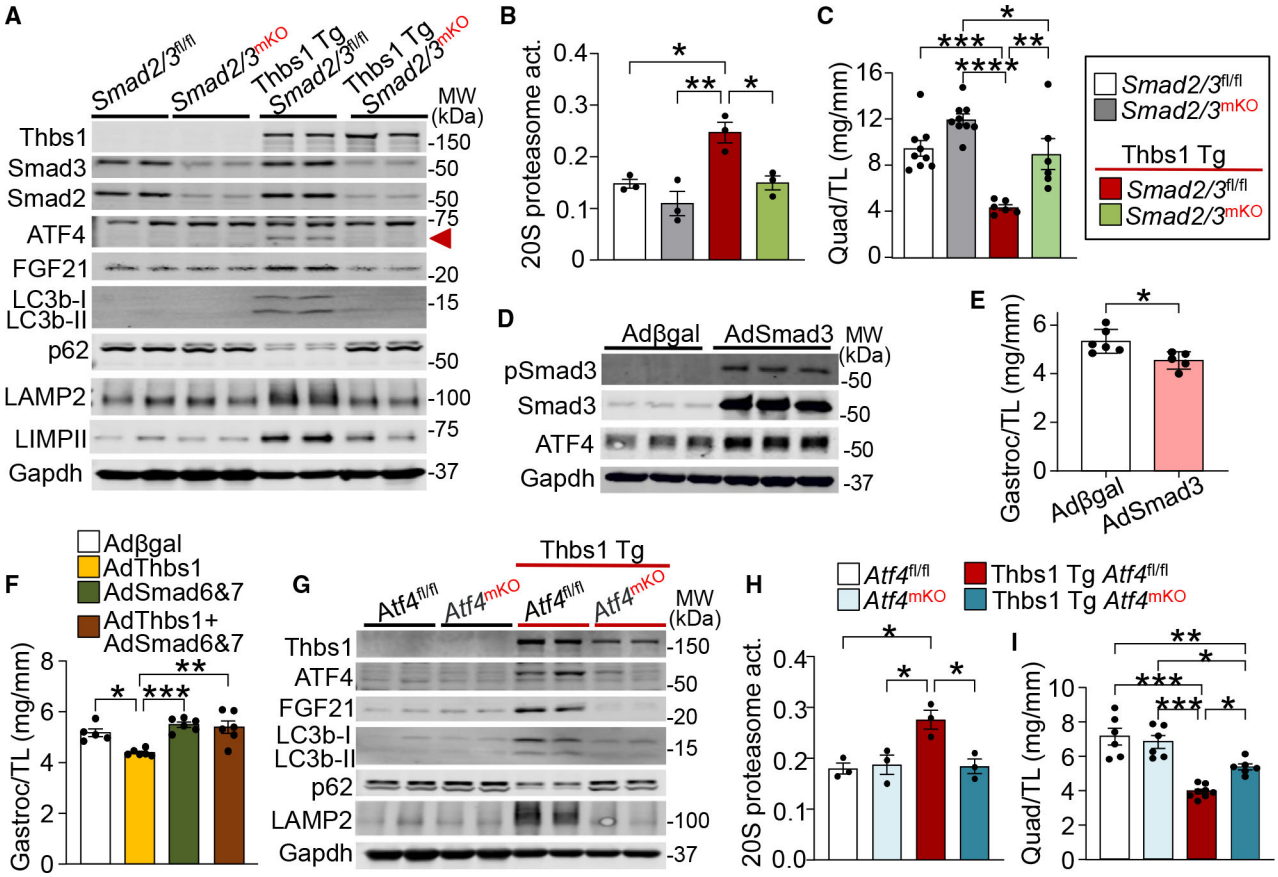

Figure 6. Canonical TGFβ effector Smad2/3 and downstream ATF4 mediate Thbs1-induced muscle atrophy

(A) Representative western blot analysis of Thbs1, Smad3, Smad2, ATF4, FGF21, LC3b, p62, LAMP2, and LIMPII in 12-week-old quadriceps protein extracts from *Smad2/3*$^{fl/fl}$, *Smad2/3*$^{fl/fl}$-*Myl1*-Cre (*Smad2/3*^{mKO}), Thbs1 Tg *Smad2/3*$^{fl/fl}$, and Thbs1 Tg *Smad2/3*^{mKO} mice. Gapdh serves as loading control; $n = 2$ biologically independent animals per genotype. Red arrowhead indicates ATF4.

(B and C) 20S chymotrypsin-like proteasome activity (pmol/[min·μg]; B) and quadriceps (Quad) weight normalized to tibia length (TL; C) from the indicated genotypes of mice at 12 weeks of age based on the color-coded legend shown on the right. Error bars denote ±SEM. The number of biologically independent animals per genotype are indicated in the graphs. *$p < 0.05$, **$p < 0.01$, ***$p < 0.001$, ****$p < 0.0001$ by one-way ANOVA and Tukey's multiple comparison test.

(D) Western blots for phospho-Smad3 (Ser423/425), total Smad3, and ATF4 in gastrocnemius from 16-day-old rat pups injected with Adβgal or AdSmad3 on postnatal day 2, followed by a second "boost" injection 72 h later (3E8 viral particles per injection). Gapdh serves as loading control; $n = 3$ biologically independent animals per genotype.

(E and F) Gastrocnemius (Gastroc) weight normalized to tibia length (TL) from 16-day-old rat pups injected with Adβgal or AdSmad3 (E) or injected with Adβgal, AdThbs1, AdSmad6, and/or AdSmad7 (F), following the timeline described for (D) (all 3E8 viral particles per injection). Error bars denote ±SEM from $n = 5$–6 biologically independent

animals per treatment group. *$p < 0.05$ by two-tailed unpaired Student's t test for (E); *$p < 0.05$, **$p < 0.01$, ***$p < 0.001$ by one-way ANOVA and Tukey's multiple comparison test for (F).

(G) Western blot analysis for Thbs1, ATF4, FGF21, LC3b, p62, LAMP2, and Gapdh in 12-week-old quadriceps protein extracts from *Atf4*$^{fl/fl}$, *Atf4*$^{fl/fl}$-*Myl1*-Cre (*Atf4*^{mKO}), Thbs1 Tg *Atf4*$^{fl/fl}$, and Thbs1 Tg *Atf4*^{mKO} mice; $n = 2$ biologically independent animals per genotype.

(H and I) 20S chymotrypsin-like proteasome activity (pmol/[min·μg]; H) and quadriceps (Quad) weight normalized to tibia length (TL; I) from the indicated genotypes at 12 weeks of age. Error bars denote ±SEM from $n = 3$ biologically independent animals per genotype in (H) and $n = 6–8$ biologically independent animals per genotype for (I). *$p < 0.05$, **$p < 0.01$, ***$p < 0.001$, by one-way ANOVA and Tukey's multiple comparison test.

See also Figure S7.

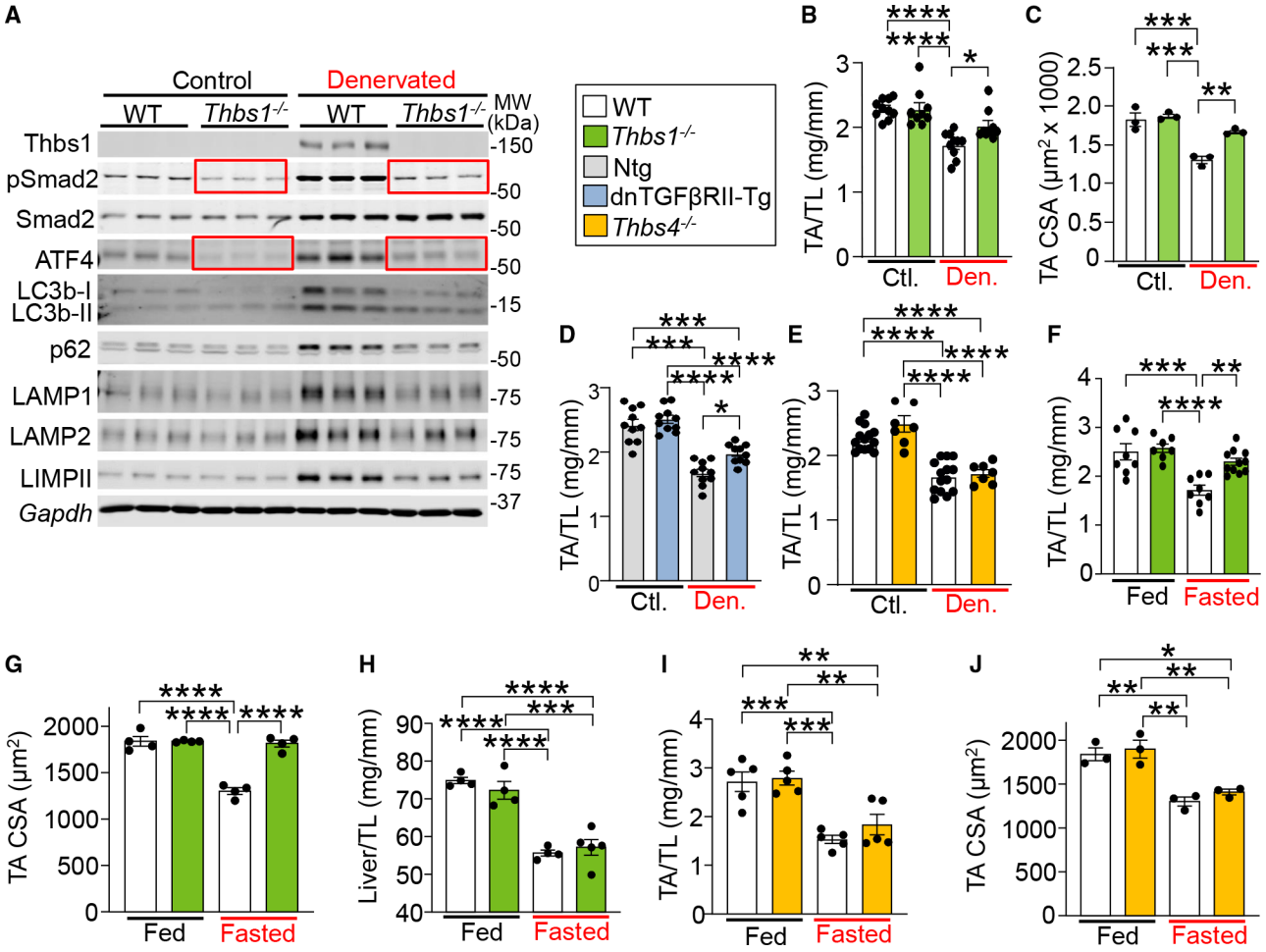

Figure 7. Loss of *Thbs1* blunts muscle atrophy induced by denervation and fasting

(A) Representative western blot analysis of phospho-Smad2 (Ser465/467), total Smad2, ATF4, LC3b, p62, LAMP1, LAMP2, LIMPII, and Gapdh control in the tibialis anterior (TA) of wild-type (WT) and *Thbs1*$^{-/-}$ mice subjected to 10 days of unilateral hindlimb denervation, compared to the sham-operated control contralateral TAs from the same mice. (B–E) Tibialis anterior (TA) weight normalized to tibia length (TL; B, D, and E) and TA myofiber cell surface area (CSA; C) after 10 days of denervation (Den.) in the indicated lines of mice, as compared to the non-denervated contralateral muscle (Ctl.) in the same mice. The legend to the left of (B) refers to all panels in the figure. Error bars denote ±SEM. The number of biologically independent animals per genotype are indicated in the graphs. *$p < 0.05$, **$p < 0.01$, ***$p < 0.001$, ****$p < 0.0001$ by two-tailed unpaired Student's t test. (F–J) Tibialis anterior (TA) weight normalized to tibia length (TL; F and I), TA myofiber cell surface area (CSA; G and J), and liver weight normalized to TL (H) from 8-week-old mice of indicated genotypes shown in the legend to the left of (B), which were fed *ad libitum* or fasted for 48 h. Error bars denote ±SEM. The number of biologically independent animals per genotype are indicated in the graphs. *$p < 0.05$, **$p < 0.01$, ***$p < 0.001$, ****$p < 0.0001$ by one-way ANOVA and Tukey's multiple comparison test.

KEY RESOURCES TABLE

REAGENT or RESOURCE	SOURCE	IDENTIFIER
Antibodies		
Goat polyclonal anti-Thbs1	R&D Systems	Cat# AF3074; RRID:AB_221958
Mouse monoclonal anti-Thbs1	Thermo Scientific	Cat# MA5–13395; RRID:AB_10982819
Mouse monoclonal anti-Thbs2	R&D Systems	Cat# MAB1635; RRID:AB_2202067
Goat polyclonal anti-Thbs4	R&D Systems	Cat# AF2390; RRID:AB_2202087
Rabbit polyclonal anti-Collagen I	Abcam	Cat# ab34710; RRID:AB_731684
Mouse monoclonal anti-Embryonic Myosin Heavy Chain	Developmental Studies Hybridoma Bank (DSHB)	Cat# F1.652; RRID:AB_528358
Rat monoclonal anti-Laminin	Sigma Aldrich	Cat# L0663; RRID:AB_477153
Rabbit monoclonal anti-ATF4 (D4B8)	Cell Signaling Technology	Cat# 11815; RRID:AB_2616025
Rabbit polyclonal anti-ATF4	LSBio (LifeSpan)	Cat# LS-B6361; RRID:AB_11042790
Rabbit polyclonal anti-ATF6α	SAB SignalWayAntibody LLC	Cat#24383; RRID: N/A
Rabbit polyclonal anti-GRP78/BiP	Sigma Aldrich	Cat# G8918; RRID:AB_477030
Rabbit polyclonal anti-Calreticulin	Cell Signaling Technology	Cat# 2891; RRID:AB_2275208
Mouse monoclonal anti-β-Dystroglycan	Developmental Studies Hybridoma Bank (DSHB)	Cat# MANDAG2 clone 7D11; RRID:AB_2211772
Goat polyclonal anti-FGF21	R&D Systems	Cat# AF3057; RRID:AB_2104611
Rabbit monoclonal anti-IRE1α	Cell Signaling Technology	Cat# 3294; RRID:AB_823545
Mouse monoclonal anti-Integrin, Beta 1D	Millipore	Millipore Cat# MAB1900; RRID:AB_94387
Rat monoclonal anti-Lamp-1	Developmental Studies Hybridoma Bank (DSHB)	Cat# 1D4B; RRID:AB_2134500
Rat monoclonal anti-Lamp-2	Developmental Studies Hybridoma Bank (DSHB)	Cat# ABL-93; RRID:AB_2134767
Rabbit monoclonal anti-LC3B (D11)	Cell Signaling Technology	Cat# 3868; RRID:AB_2137707
Rabbit polyclonal anti-p62/SQSTM1	Sigma Aldrich	Cat# P0067; RRID:AB_1841064
Rabbit monoclonal anti-LIMPII	Abcam	Cat# ab176317; RRID:AB_2620169
Rabbit monoclonal anti-PERK (C33E10)	Cell Signaling Technology	Cat# 3192; RRID:AB_2095847
Mouse monoclonal anti-alpha Sarcoglycan	Developmental Studies Hybridoma Bank (DSHB)	Cat# IVD3(1)A9; RRID:AB_2185657
Rabbit polyclonal anti-beta Sarcoglycan	Novus Biologicals	NBP1–90300; RRID:AB_11029326
Rabbit monoclonal anti-delta Sarcoglycan	Abcam	Cat# ab137101; RRID: N/A
Rabbit monoclonal anti-Smad2	Cell Signaling Technology	Cat# 5339; RRID:AB_10626777
Rabbit monoclonal anti-Smad3	Abcam	Cat# ab40854; RRID:AB_777979
Rabbit monoclonal anti-Phospho-Smad2 (Ser465/467)/Smad3 (Ser423/425)	Cell Signaling Technology	Cat# 8828; RRID:AB_2631089
Rabbit monoclonal anti-Phospho-Smad3 (Ser423/425) (C25A9)	Cell signaling Technology	Cat# 9520; RRID:AB_2193207
Mouse monoclonal anti-TGF beta RII (D-2)	Santa Cruz Biotechnology	Cat# sc-17799; RRID:AB_628348
Mouse monoclonal anti-Ubiquitin	Santa Cruz Biotechnology	Cat# sc-8017; RRID:AB_628423
Mouse monoclonal anti-GAPDH	Fitzgerald Industries International	Cat# 10R-G109a; RRID:AB_1285808
Rabbit polyclonal anti-mTOR	Cell Signaling Technology	Cat# 2972; RRID:AB_330978
Rabbit polyclonal anti-*p*-mTOR Ser2448	Cell Signaling Technology	Cat# 2971; RRID:AB_330970

REAGENT or RESOURCE	SOURCE	IDENTIFIER
Rabbit monoclonal anti-4E-BP1	Cell Signaling Technology	Cat# 9644; RRID:AB_2097841
Rabbit monolonal anti-*p*-4E-BP1 Thr37/46	Cell Signaling Technology	Cat# 2855; RRID:AB_560835
Rabbit monoclonal anti-p70 S6 Kinase (49D7)	Cell Signaling Technology	Cat# 2708; RRID:AB_90722
Rabbit polyclonal anti-p-p70 S6 Kinase Thr389	Cell Signaling Technology	Cat# 9205; RRID:AB_330944
Rabbit polyclonal anti-AMPKα	Cell Signaling Technology	Cat# 2532; RRID:AB_330331
Rabbit monoclonal anti-*p*-AMPKα Thr172	Cell Signaling Technology	Cat# 2535; RRID:AB_331250
Rabbit polyclonal anti-Akt	Cell Signaling Technology	Cat# 9272; RRID:AB_329827
Rabbit monoclonal anti-*p*-Akt Ser473	Cell Signaling Technology	Cat# 4060; RRID:AB_2315049
Rabbit monoclonal anti-Foxo1	Cell Signaling Technology	Cat# 2880; RRID:AB_2106495
Rabbit polyclonal anti-*p*-Foxo1 Ser256	Cell Signaling Technology	Cat# 9461; RRID:AB_329831
Rabbit monoclonal anti-Foxo3	Cell Signaling Technology	Cat# 2497; RRID:AB_836876
Rabbit monoclonal anti-*p*-Foxo3 Ser413	Cell Signaling Technology	Cat# 8174; RRID:AB_10889562
Rabbit polyclonal anti *p*-Foxo3 Ser253	Cell Signaling Technology	Cat# 9466; RRID:AB_2106674
Mouse monoclonal anti-Puromycin	Sigma Aldrich	Cat# MABE343; RRID:AB_2566826
Rat monoclonal anti-CD45	BD Pharmingen	Cat# 553076; RRID:AB_394606
Rabbit polyclonal anti-pSmad2/3	MaineHeatlh Institute for Research	Cat# D8591; RRID: N/A
IRdye 800CW Goat anti-Mouse	LI-COR Biosciences	Cat# 926–32210; RRID:AB_621842
IRdye 800CW Goat anti-Rabbit	LI-COR Biosciences	Cat# 926–32211; RRID:AB_621842
IRdye 800CW Goat anti-Rat	LI-COR Biosciences	Cat# 926–32219; RRID:AB_1850025
IRdye 680RD Goat anti-Mouse	LI-COR Biosciences	Cat# 926–68070; RRID:AB_10956588
IRdye 680RD Goat anti-Rabbit	LI-COR Biosciences	Cat# 926–68071; RRID:AB_10956166
IRdye 680RD Goat anti-Rat	LI-COR Biosciences	Cat# 926–68076; RRID:AB_10956590
IRdye 800CW Donkey anti-Goat	LI-COR Biosciences	Cat# 926–32214; RRID:AB_621846
IRdye 680RD Donkey anti-Goat	LI-COR Biosciences	Cat# 926–68074; RRID:AB_10956736
IRdye 680RD Donkey anti-Mouse	LI-COR Biosciences	Cat# 926–68072; RRID:AB_10953628
Bacterial and virus strains		
AdThbs1	Lynch et al.[22]	N/A
AdThbs1Δt1	This paper	N/A
AdSmad6	Accornero et al.[48]	N/A
AdSmad7	Accornero et al.[48]	N/A
AdSmad3	This paper	N/A
Ad-eGFP-tagged VSVG-ts045	Vanhoutte et al.[24]	N/A
Adcre recombinase	Khalil et al.[64]	N/A
Adβgal	Accornero et al.[48]	N/A
MyoAAV-Thbs1	This paper	N/A
MyoAAV-Luciferase	Jiuzhou Huo et al.[65]	N/A
CellLight™ Golgi-RFP Bacmam 2.0	Thermo Fisher	Cat# C10593
Chemicals, peptides, and recombinant proteins		

REAGENT or RESOURCE	SOURCE	IDENTIFIER
Trypsin-EDTA, 0.25%	Fisher Scientific	Cat# MT25–053-Cl
Bovine Growth Serum	Fisher Scientific	Cat# SH3054103
DMEM/High Glucose	Fisher Scientific	Cat# SH30022.01
Hyclone Medium 199/EBSS	Fisher Scientific	Cat# SH30253FS
Penicillin-Streptomycin	Corning Life Sciences	Cat# 30–0002-CI
Recombinant mouse TGFβ1	R&D Systems	Cat# 7666-MB-005
Paraformaldehyde, 32%	Electron Microscopy Sciences	Cat# 15714
Tissue-Tek® O.C.T.	Sakura Finetek	Cat# 4583
Normal goat serum	Jackson ImmunoResearch Laboratories	Cat# 017–000-121
Normal Donkey serum	Jackson ImmunoResearch Laboratories	Cat# 005–000-121
Antigen retrieval CITRA	BioGenex	Cat# HK086–9K
biotinylated Isolectin B4	Vector Laboratories	Cat# B-1205)
Triton® X-100	Sigma Aldrich	Cat# T8787
Lectin from Triticum Vulgaris (Wheat)	Millipore Sigma	Cat# L4895
WGA-Alexa Fluor-594	Thermo Fisher	Cat# W11262
ProLong™ Diamond antifade mountant with DAPI	Thermo Fisher	Cat# p36971
SsoAdvanced Universal SYBR Green Supermix	Bio-Rad	Cat# 1725274
Puromycin	Thermo Fisher	Cat# A113803
Colchicine	Sigma Aldrich	Cat# C9754
Cycloheximide solution	Sigma-Aldrich	Cat# C4859; CAS: 66–81-9
Ultrostain 2	Thermo Fisher	Cat# NC1936447
Halt™ Protease and Phosphatase single-use inhibitor cocktail	Thermo Scientific	Cat# 78442
Immobilon®-FL PVDF membrane	Millipore	Cat# IPFL00010
Immobilon®-PSQ PVDF membrane	Millipore	Cat# ISEQ20200
Tween 20	Fisher Scientific	Cat# BP337–500
phosphoBLOCKER™ blocking reagent	Cell Biolabs, Inc.	Cat# AKR-104
Ponceau S solution	Sigma Aldrich	Cat# P7170
InstantBlue® Coomassie protein stain	Abcam	Cat# Ab119211
Critical commercial assays		
RNeasy Fibrous Tissue Kit	Qiagen	Cat# 74704
SuperScript™ First-Strand Synthesis System	Invitrogen	Cat# 18080051
ELISA kit for Thbs1	Uscn Life Science	Cat# SEA611Mu
TGF-beta 1 Quantikine ELISA kit	R&D Systems	Cat# SMB100B
Proteasome Activity Assay Kit	Abcam	Cat# ab107921
Embed 812 Embedding Kit with BDMA	Electron Microscopy Sciences	Cat# 14121
Compartment Protein Extraction Kit	Millipore	Cat# 2145
In-Fusion® HD cloning kit	Takara Bio	Cat# 639649
Deposited data		
Gene Expression Omnibus	Gambara G. et al.[60]	GEO: GSE80223

REAGENT or RESOURCE	SOURCE	IDENTIFIER
Gene Expression Omnibus	This manuscript	GEO: GSE245663
Experimental models: Primary Cell lines		
Eif2ak3$^{fl/fl}$ mouse embryonic fibroblasts	This manuscript	N/A
C57Bl/6J mouse embryonic fibroblasts	This manuscript	N/A
Neonatal rat ventricular myocytes	This manuscript	N/A
Experimental models: Organisms/strains		
Mouse: Ska-Thbs1 Tg	Lynch et al.[22]	N/A
Mouse: Tg(ACTA1-Thbs4)2Jmol/J	Lynch et al.[22]	RRID:IMSR_JAX:036161
Mouse: Tg(ACTA1-Atf6)3Jmol/J	Vanhoutte et al.[24]	RRID:IMSR_JAX:036160
Mouse: Ska-dnTGFBRII Tg	Accornero et al.[48]	N/A
Mouse: Ska-Thbs2 Tg	This manuscript	N/A
Mouse: *B6.129S2-Thbs1tm1Hyn/J*	The Jackson Laboratory	RRID:IMSR_JAX:006141
Mouse: B6.129P2-Thbs4tm1Dgen/J	The Jackson Laboratory	RRID:IMSR_JAX:005845
Mouse: *B6.129S1-Cd36tm1 Mfe/J*	The Jackson Laboratory	RRID:IMSR_JAX:019006
Mouse: *B6.129S7-Cd47tm1Fpl/J*	The Jackson Laboratory	RRID:IMSR_JAX:003173
Mouse: *Eif2ak3tm1.2Drc/J*	The Jackson Laboratory	RRID:IMSR_JAX:023066
Mouse: *Atf6*-null	Yamamoto et al.[62]	N/A
Mouse: *Smad2* lox/lox	Park et al.[31]	N/A
Mouse: *Smad3* lox/lox	Park et al.[31]	N/A
Mouse: *Atf4* lox/lox	Ebert et al.[17]	N/A
Mouse: *Myl1tm1(cre)Sjb/J*	The Jackson Laboratory	RRID:IMSR_JAX:024713
Mouse: *C57BL/6J*	The Jackson Laboratory	RRID:IMSR_000664
Mouse: Sgcd-null (δ-Sarcoglycan)	Hack et al.[63]	N/A
Rat: Sprague-Dawley rats	Inotiv	Cat# 002
Oligonucleotides		
Primer: *SalI*-Thbs2 Forward GTCGACATGCTCTGGGCACTGGCC	Invitrogen	N/A
Primer: *SalI*-Thbs2 Reverse GTCGACCTAGGCATCTCTGCACTCATACTTG	Invitrogen	N/A
qPCR primers; see Table S1	Invitrogen	N/A
Recombinant DNA		
MGC Mouse Thbs2 cDNA	Horizon Discovery	Cat# MMM1013–202702786 Clone Id: 3583417
pShuttle-CMV Vector	Agilent	Cat# 240007
MyoAAV vector	Tabebordbar et al.[66]	N/A
pAAV-MCS vector	Cell biolabs	Cat# VPK-410
Software and algorithms		
NIS Elements	Nikon Instruments Inc.	RRID:SCR_014329

REAGENT or RESOURCE	SOURCE	IDENTIFIER
ImageJ	Schneider et al.[67]	RRID:SCR_003070
LI-COR Image Studio Software	LI-COR Biosciences	RRID:SCR_015795
DESeq	Bioconductor	RRID:SCR_000154
Prism 9.5.0 (730)	GraphPad	RRID:SCR_002798
BioRender	BioRender	RRID:SCR_018361
Other		
Nikon A1 confocal Laser Microscope	Nikon Instruments Inc.	RRID:SCR_020318
Bio-Rad CFX96 Real-Time PCR Detection System	Bio-Rad	RRID:SCR_018064
Fisherbrand™ 150 homogenizer	Fischer Scientific	Cat# 15–340-168
Biomasher II Closed System Micro Tissue Homogenizer	DWK Life Sciences Kimble™	Cat# 749625–0010
Direct Detect® Spectrometer	Millipore Sigma	Cat# C134681
Direct Detect® assay-free cards	Millipore Sigma	Cat# DDAC00010–8P
Amicon ultra-4 centrifugal filter devices	Millipore	Cat# UFC810024